mL, 50 min) or soluble TNF receptor I (1 and 10 ng/mL, 50 min) significantly inhibited the TNF-α-induced increase in [^{3}H] DA uptake ($F_{5,34}$ = 7.370 for anti-TNF-α antibody; $F_{5,34}$ = 7.526 for soluble TNF receptor I, $p < 0.01$, one-way ANOVA) (Fig. 1b and c), although the anti-TNF-α antibody (10, 50, and 100 ng/mL, 50 min) or soluble TNF receptor I (1 and 10 ng/mL, 50 min) itself had no effect on DA uptake (Fig. 1d). These results suggest that TNF-α activates DA uptake in PC12 cells.

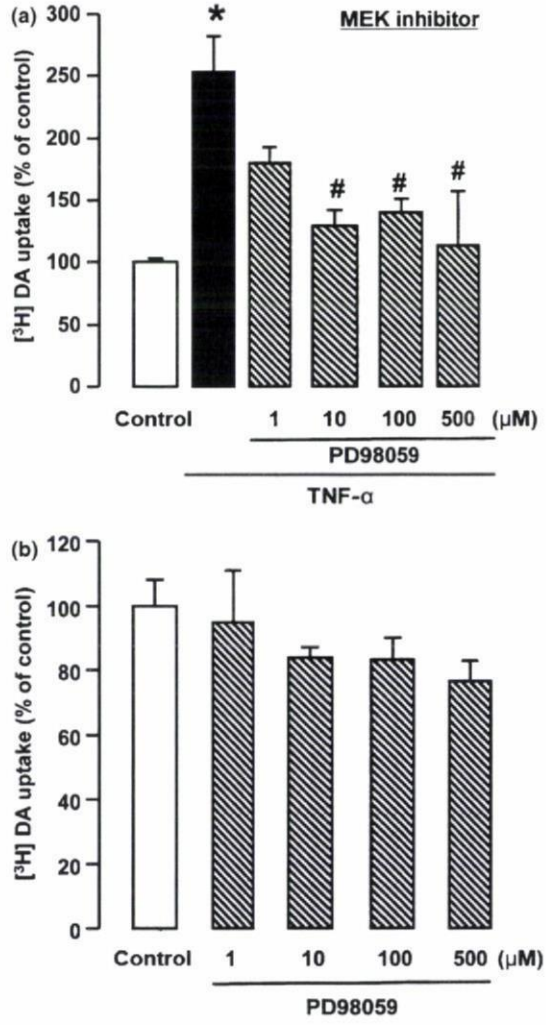

Fig. 2 Effects of MEK inhibitor on TNF-α-induced increase in [^{3}H] DA uptake in PC12 cells. (a) Effects of the MEK inhibitor PD98059 on TNF-α-induced increase in [^{3}H] DA uptake in PC12 cells. The cells were pre-treated with PD98059 (1, 10, 100, and 500 μM) 10 min before their treatment with TNF-α (10 ng/mL, 40 min), and assayed for [^{3}H] DA uptake. The [^{3}H] DA uptake was 0.10 ± 0.00 pmol/10 min for control. The final concentration of [^{3}H] DA was 20 nM. Values are means ± SE (n = 4). *$p < 0.05$ versus control. #$p < 0.05$ versus TNF-α-treated cells. (b) Effects of PD98059 on [^{3}H] DA uptake in PC12 cells. The cells were pre-treated with PD98059 (1, 10, 100, and 500 μM) for 50 min, and assayed for [^{3}H] DA uptake. The [^{3}H] DA uptake was 0.12 ± 0.00 pmol/10 min for the control. The final concentration of [^{3}H] DA was 20 nM. Values are means ± SE (n = 4).

Effects of mitogen-activated protein kinase kinase inhibitor on TNF-α-induced increase in DA uptake in PC12 cells

TNF-α modulates cellular responses through the ERK1/2 signaling pathway (van Vliet *et al.* 2005). Therefore, we investigated whether the TNF-α-induced increase in DA

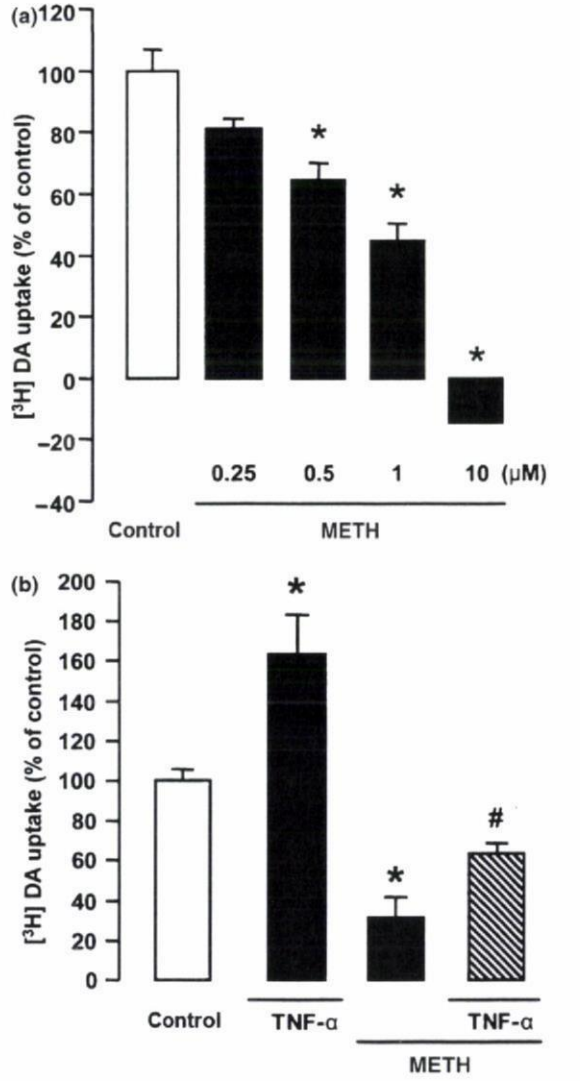

Fig. 3 Effects of TNF-α on METH-induced decrease in [^{3}H] DA uptake in PC12 cells. (a) Dose-response effects of METH on [^{3}H] DA uptake in PC12 cells. The cells were pre-treated with METH (0.25, 0.5, 1, and 10 μM) for 30 min, and assayed for [^{3}H] DA uptake. The [^{3}H] DA uptake was 0.28 ± 0.02 pmol/10 min for the control. The final concentration of [^{3}H] DA was 20 nM. Values are means ± SE (n = 4). *$p < 0.05$ versus control. (b) Effects of TNF-α on METH-induced decrease in [^{3}H] DA uptake in PC12 cells. The cells were pre-treated with TNF-α (10 ng/mL) 10 min before being treated with METH (1 μM, 30 min), and assayed for [^{3}H] DA uptake. The [^{3}H] DA uptake was 0.19 ± 0.01 pmol/10 min for the control. The final concentration of [^{3}H] DA was 20 nM. Values are means ± SE (n = 5). *$p < 0.05$ versus control. #$p < 0.05$ versus METH-treated cells.

uptake was antagonized by the MEK inhibitor PD98059 in PC12 cells.

Pre-treatment with PD98059 (10, 100, and 500 μM, 50 min) significantly inhibited the TNF-α-induced increase in [^{3}H] DA uptake ($F_{5,18} = 5.961$, $p < 0.01$, one-way ANOVA) (Fig. 2a), although PD98059 (1, 10, 100, and 500 μM, 50 min) itself had no effect on the uptake (Fig. 2b). These results suggest that TNF-α activates DA uptake via the MEK signaling pathway in PC12 cells.

Effects of TNF-α on METH-induced decrease in DA uptake in PC12 cells

We have previously demonstrated that TNF-α and its inducer diminish the METH-induced decrease in DA uptake and inhibit the rewarding effects of and sensitization to METH (Nakajima *et al.* 2004; Niwa *et al.* 2007c, e). Therefore, we confirmed the effects of TNF-α on the METH-induced decrease in DA uptake in PC12 cells.

METH (0.5, 1, and 10 μM, 30 min) decreased [^{3}H] DA uptake compared with the control group in a dose-dependent manner ($F_{4,15} = 83.675$, $p < 0.01$, one-way ANOVA) (Fig. 3a). Moreover, TNF-α (10 ng/mL, 40 min) inhibited the METH-induced decrease in [^{3}H] DA uptake (TNF-α, $F_{1,16} = 14.759$, $p < 0.01$; METH, $F_{1,16} = 45.994$, $p < 0.01$; TNF-α·METH $F_{1,16} = 1.573$, $p = 0.228$; two-way ANOVA) (Fig. 3b). These results suggest that TNF-α inhibits the METH-induced decrease in DA uptake in PC12 cells (Fig. 3) as well as promoting plasmalemmal and vesicular DA uptake to diminish METH and morphine-induced behavioral sensitization and rewarding effects (Nakajima *et al.* 2004; Niwa *et al.* 2007b; Niwa *et al.* 2008).

Transfection of the vector containing shati cDNA into PC12 cells

We established a PC12 cell line transfected with the vector containing shati cDNA to examine the role of shati in DA uptake and the METH-induced decrease in DA uptake.

We used immunostaining for TH to check morphological changes of the PC12 cells after the transfection of the vector containing shati cDNA. Morphological changes to the cells were not observed after the transfection compared with mock-transfected or non-transfected PC12 cells (Fig. 4a). To confirm the transfection of the vector containing shati cDNA, we checked for immunostaining against S-4 and GFP, co-expressed with shati. No immunoreactivity for S-4 or GFP was found in the cells that were mock-transfected, which express neither shati nor GFP [Fig. 4b (i)]. The cells mock-transfected (=expression vector [pcDNA-DEST53]), which express GFP, but not shati, were immunopositive for GFP, but not S-4 [Fig. 4b (ii)]. The cells transfected with the vector containing shati cDNA, which express both shati and GFP, were immunopositive for S-4 and GFP [Fig. 4b (iii)]. The cells immunopositive for S-4 were merged with those positive for GFP. These results indicated that shati was certainly expressed in PC12 cells and transfection did not affect cell survival or morphology.

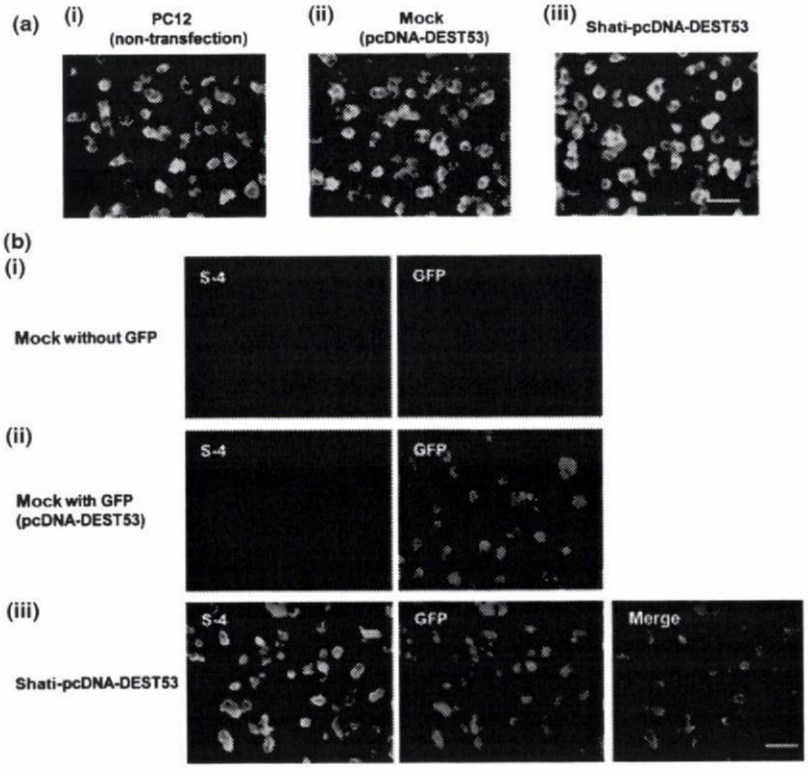

Fig. 4 Transfection of the vector containing shati cDNA into PC12 cells. (a) The morphological changes of the PC12 cells after transfection of the expression vector (pcDNA-DEST53) (ii) or vector containing shati cDNA (iii). The expression vector alone (mock-transfection) (ii), or the vector containing shati cDNA (iii) was introduced into PC12 cells. There were no changes in survival or morphology in the transfected PC12 cells. Scale bar: 20 μm. (b) Immunostaining of shati in PC12 cells transfected with the vector containing shati cDNA. pENTR/TEV/D-TOPO (without shati recombination and green fluorescent protein (GFP) site) (i), pcDNA-DEST53 with GFP (mock-transfection) (ii), or the vector containing shati cDNA and GFP (iii), was introduced into PC12 cells. The shati-immunopositive cells (green) were colocalized with GFP-immunopositive cells (red). Double immunostaining for S-4 and GFP in PC12 cells transfected with the vector containing shati cDNA reveals overexpression of shati in PC12 cells (iii). Scale bar: 20 μm.

Effect of over-expressed shati on DA uptake in PC12 cells

We have previously demonstrated that shati-AS, which inhibits the expression of shati mRNA, significantly potentiates the METH-induced decrease in synaptosomal and vesicular [^{3}H] DA uptake compared with that in the shati-SC or CSF-treated mice (Niwa *et al.* 2007a). Moreover, [^{3}H] DA uptake in saline-treated mice was also decreased by shati-AS compared with that in the CSF-treated mice, although shati-SC had no effect on [^{3}H] DA uptake (Niwa *et al.* 2007a). Given the results for synaptosomal and vesicular [^{3}H] DA uptake using shati-AS, we concluded that shati plays a critical role in modulating DA uptake. To address this issue, we investigated the role of shati in DA uptake in PC12 cells transfected with the vector containing shati cDNA.

Transfection of the vector containing shati cDNA increased shati mRNA expression compared with the mock-transfection, suggesting that shati was over-expressed in these cells (Fig. 5a left two columns). The increase in the levels of shati mRNA expression evoked by METH treatment (1 μM, 30 min) in mock-transfected cells was significantly potentiated by shati over-expression in PC12 cells (drug, $F_{1,28} = 20.917$, $p < 0.01$; transfection, $F_{1,28} = 247.684$, $p < 0.01$; drug × transfection, $F_{1,28} = 0.003$, $p = 0.955$; two-way ANOVA) (Fig. 5a right two columns).

We examined the *in vitro* effect of over-expressed shati on [^{3}H] DA uptake in PC12 cells. Shati-over-expressing cells themselves showed increased [^{3}H] DA uptake compared with the mock-transfected cells, suggesting that shati itself promotes DA uptake (Fig. 5b left two columns). We pre-treated PC12 cells with METH (1 μM) for 30 min, and then assayed the uptake of [^{3}H] DA. As shown in Fig. 5b, METH (1 μM, 30 min) decreased [^{3}H] DA uptake compared with the mock-transfected control cells. In the shati-over-expressing cells, the METH-induced decrease in [^{3}H] DA uptake was significantly inhibited compared with that in the mock-transfected cells (drug, $F_{1,40} = 45.807$, $p < 0.01$; transfection, $F_{1,28} = 21.551$, $p < 0.01$; drug × transfection, $F_{1,28} = 0.001$, $p = 0.971$; two-way ANOVA) (Fig. 5b right two columns). These results indicated that shati could attenuate METH-induced inhibition of DA uptake.

Regulation of TNF-α expression by shati

TNF-α activates synaptosomal and vesicular DA uptake (Nakajima *et al.* 2004). TNF-α and its inducer diminish the METH-induced decrease in DA uptake and inhibit the METH-induced dependence (Nakajima *et al.* 2004; Niwa *et al.* 2007c, e). Moreover, given the findings on [^{3}H] DA uptake obtained using shati-AS (Niwa *et al.* 2007a) and shati-over-expressing cells (Fig. 5b), we hypothesized that shati increased DA uptake by regulating TNF-α. To address this issue, we examined expression levels of TNF-α mRNA after transfection of the vector containing shati cDNA or treatment with shati-AS.

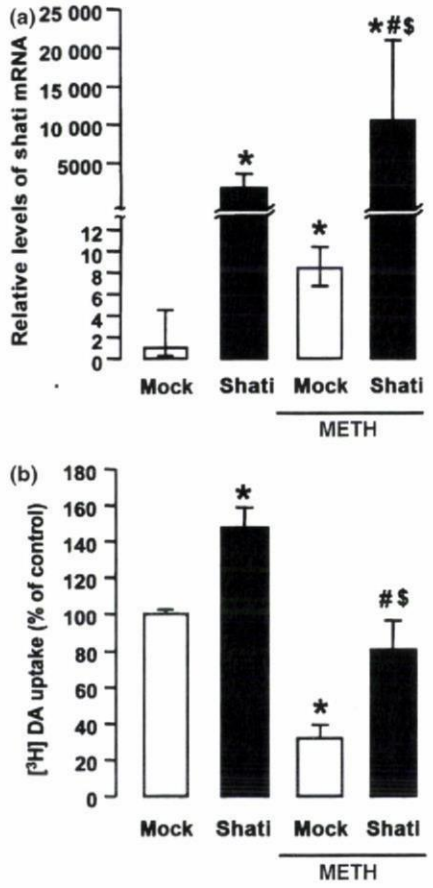

Fig. 5 Effect of overexpression of shati on DA uptake in PC12 cells. (a) Shati mRNA expression in PC12 cells transfected with the vector containing shati cDNA. The mock construct (pcDNA-DEST53), or the vector containing shati cDNA was introduced into PC12 cells. These cells were treated with 1 μM METH for 30 min. Values are means ± SE ($n = 8$). $^*p < 0.05$ versus mock-transfected cells. $^\#p < 0.05$ versus the vector containing shati cDNA-transfected cells. $^\$p < 0.05$ versus METH + mock-transfected cells. (b) Effect of over-expression of shati on [^{3}H] DA uptake in PC12 cells. The mock construct (pcDNA-DEST53), or the vector containing shati cDNA was introduced into PC12 cells. The cells were pre-treated with 1 μM METH for 30 min, and [^{3}H] DA uptake was measured. The [^{3}H] DA uptake was 0.12 ± 0.02 pmol/10 min for the mock-transfected cells. The final concentration of [^{3}H] DA was 20 nM. Values are means ± SE ($n = 10$–12). $^*p < 0.05$ versus mock-transfected cells. $^\#p < 0.05$ versus the vector containing shati cDNA-transfected cells. $^\$p < 0.05$ versus METH + mock-transfected cells.

Shati-over-expressing cells themselves had increased TNF-α mRNA expression compared with the mock-transfected cells (Fig. 6a left two columns), suggesting that shati regulates expression of TNF-α in PC12 cells. The increase in TNF-α mRNA expression evoked by METH treatment (1 μM, 30 min) in mock-transfected cells was significantly potentiated by overexpression of shati *in vitro* (drug, $F_{1,28} = 21.000$, $p < 0.01$; transfection, $F_{1,28} = 65.860$,

$p < 0.01$; drug × transfection, $F_{1,28} = 3.557$, $p = 0.070$; two-way ANOVA) (Fig. 6a right two columns). As shown in Fig. 6b right three columns, the increase in TNF-α mRNA expression evoked by repeated METH treatment in the NAc was significantly abolished by shati-AS, although shati-SC had no effect. Moreover, TNF-α mRNA expression in the NAc of saline-treated mice was also inhibited by shati-AS, although not by shati-SC (drug, $F_{1,47} = 48.473$, $p < 0.01$; intracerebroventricular treatment, $F_{2,47} = 15.670$, $p < 0.01$; drug × intracerebroventricular treatment, $F_{2,47} = 0.239$, $p = 0.788$; two-way ANOVA) (Fig. 6b left three columns), indicating that shati-AS decreases effectively the expression of TNF-α mRNA through the down-regulation of shati mRNA expression.

As shown in Fig. 6c, right four columns, the ameliorative effect of shati on the METH-induced decrease in DA uptake

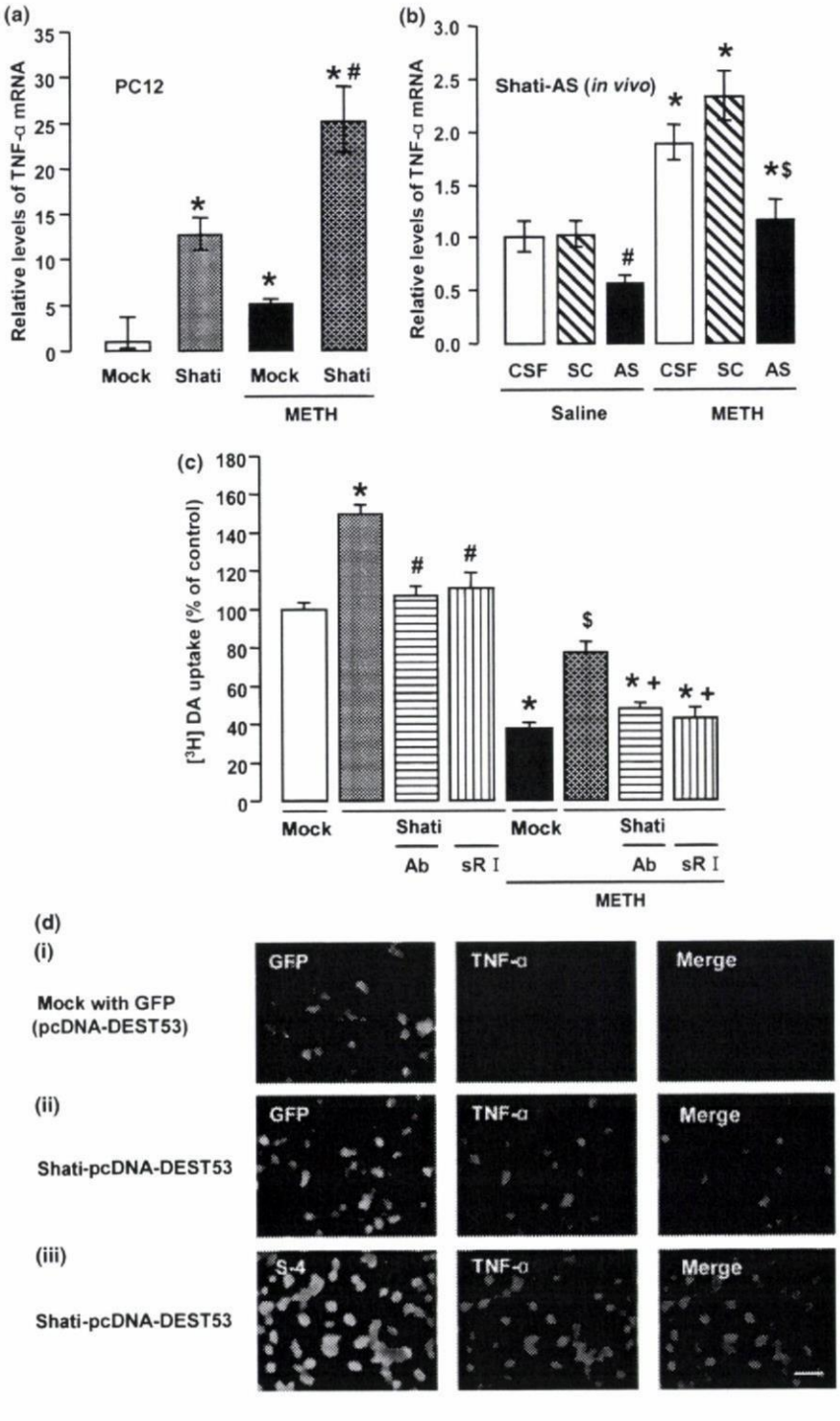

was antagonized by treatment with the TNF-αantibody (50 ng/mL) or soluble TNF receptor I (1 ng/mL). The shati-induced potentiation of DA uptake was also inhibited by the treatments in shati-over-expressing cells (drug, $F_{1,72} = 296.090$, $p < 0.01$; transfection, $F_{1,72} = 13.864$, $p < 0.01$; neutralization, $F_{1,72} = 32.930$, $p < 0.01$; drug × transfection, $F_{1,72} = 0.189$, $p = 0.665$; drug × neutralization, $F_{1,72} = 1.496$, $p = 0.225$; transfection × neutralization, $F_{1,72} = 34.828$, $p < 0.01$; drug × transfection × neutralization, $F_{1,72} = 0.003$, $p = 0.958$; three-way ANOVA) (Fig. 6c left four columns). These results suggest that over-expression of shati increased DA uptake by regulating TNF-α in PC12 cells. To confirm the relationship between shati and TNF-α, we examined immunostaining for GFP, which is co-expressed with shati, or S-4 and TNF-α. The cells mock-transfected, which express GFP, but not shati, were immunopositive for GFP, but not TNF-α. The cells transfected with the vector containing shati cDNA, which express both GFP and shati, were immunopositive for GFP or S-4 and TNF-α. The cells immunopositive for S-4 were merged with those positive for TNF-α. These results indicated that shati was expressed in TNF-α-immunopositive cells (Fig. 6d).

Discussion

DA is the predominant catecholamine neurotransmitter in the CNS. Disruptions of DA signaling contribute to various psychiatric and neurological disorders, including drug addiction, schizophrenia, and Parkinson's disease (Self and Nestler 1995; Hyman 1996). Extracellular DA levels are primarily regulated by DAT, an integral membrane protein that is a member of the Na^+/Cl^--dependent co-transporter gene family (Amara and Kuhar 1993). By removing extracellular DA and recycling it back to the neuron, DAT plays an essential role in terminating DA signaling. Pharmacological blockage of DAT by psychostimulants inhibits the reuptake of DA from the extracellular space, resulting in increased extracellular DA levels and augmented receptor stimulation (Horn 1990). Although pharmacological and genetic ablation (Grace 1995; Jones *et al.* 1998) studies indicate a critical role for DAT in the maintenance of DA neuronal homeostasis, the endogenous mechanisms regulating DAT expression and activity are poorly understood.

The PC12 cell line is derived from the rat pheochromocytoma. It is often used as an *in vitro* model to understand the physiology of central DA neurons (Roda *et al.* 1980; Tischler 2002; Fornai *et al.* 2007). A number of factors contribute to the wide use of PC12 cells: they are inexpensive as well as easy to handle, and mimic many features of central DA neurons. In fact, PC12 cells produce catecholamines (Markey *et al.* 1980; Roda *et al.* 1980; Vaccaro *et al.* 1980). In particular, they contain DA (Greene and Rein 1978) as the main catecholamine and bear DA receptors on their external membrane (Sampath *et al.* 1994). In light of the presence of DA and DA receptors, as well as DA uptake mechanisms, PC12 cell lines are considered to be closer to DA terminals than their ancestors (i.e. chromaffin cells of the adrenal medulla). This concept is reinforced by the presence of monoamine oxidase type A, which also characterizes DA neurons (Finberg and Youdim 1983), in contrast with the established prevalence of monoamine oxidase type B within chromaffin cells of the adrenal medulla (Youdim 1991).

Recently, we have demonstrated that TNF-α and its inducer play a neuroprotective role in the behavioral sensitization to and rewarding effects of METH by activating plasmalemmal and vesicular DAT as well as by inhibiting the METH-induced increase in extracellular DA levels (Nakajima *et al.* 2004; Niwa *et al.* 2007c,e). TNF-α modulates cellular responses through the ERK1/2 and NF-κB signaling pathways (van Vliet *et al.* 2005). The adaptor protein TNF receptor-associated factor 2 (TRAF2) and the serine and threonine protein kinase receptor-interacting protein are required for optimal TNF-induced signaling through ERK1/2, c-Jun N-termial kinase (JNK) and p38 mitogen-activated

Fig. 6 Involvement of TNF-α in shati-induced increase in DA uptake in PC12 cells. (a) TNF-α mRNA expression in PC12 cells transfected with the vector containing shati cDNA. The expression vector alone (pcDNA-DEST53), or the vector containing shati cDNA was introduced into PC12 cells. The cells were treated with 1 μM METH for 30 min. Values are means ± SE ($n = 8$). $^*p < 0.05$ versus mock-transfected group. $^\#p < 0.05$ versus METH + mock-transfected group. (b) Effect of shati-AS on TNF-α mRNA expression. Mice were administered METH (1 mg/kg, s.c.) for 5 days and decapitated 2 h after the final treatment. Values are means ± SE ($n = 8$–10). $^*p < 0.05$ versus corresponding saline-treated mice. $^\#p < 0.05$ versus saline + CSF and saline + shati-SC-treated mice. $^\$p < 0.05$ versus METH + CSF and METH + shati-SC-treated mice. (c) Involvement of TNF-α in shati-induced increase in [^{3}H] DA uptake in PC12 cells. The expression vector alone (pcDNA-DEST53), or the vector containing shati cDNA was introduced into PC12 cells. The cells were pre-treated with anti-TNF-α antibody (Ab; 50 ng/mL) or soluble TNF receptor I (sR I; 1 ng/mL) 10 min before their treatment with METH (1 μM, 30 min), and assayed for [^{3}H] DA uptake. The [^{3}H] DA uptake was 0.15 ± 0.02 pmol/10 min for the mock-transfected group. The final concentration of [^{3}H] DA was 20 nM. Values are means ± SE ($n = 10$). $^*p < 0.05$ versus mock-transfected group. $^\#p < 0.05$ versus the vector containing shati cDNA-transfected group. $^\$p < 0.05$ versus METH + mock-transfected group. $^+p < 0.05$ versus METH + the vector containing shati cDNA-transfected group. (d) Immunostaining of shati and TNF-α in PC12 cells transfected with the vector containing shati cDNA. The expression vector alone (pcDNA-DEST53) (i), or the vector containing shati cDNA (ii) (iii) was introduced into PC12 cells. The GFP or shati-immunopositive cells (green) were co-localized with TNF-α-immunopositive cells (red) (ii) (iii). Double immunostaining for GFP or S-4 and TNF-α in PC12 cells transfected with the vector containing shati cDNA reveals expression of shati in TNF-α-immunopositive cells (ii) (iii). Scale bar: 20 μm.

protein kinase (p38) (Baud and Karin 2001; Devin *et al.* 2003). MEK inhibitor PD98059 significantly decreases phosphorylated ERK1/2 without affecting total ERK level, MEK-JNK, -p38, and -NF-κB, resulting in loss of DAT surface expression and DAT capacity. According these results, MEK-ERK pathway, but not MEK-JNK, -p38, or -NF-κB pathway, is important for intracellular trafficking and transport capacity of DAT (Morón *et al.* 2003). Therefore, we investigated the involvement of TNF-α in DA uptake and the METH-induced inhibition of DA uptake in PC12 cells. Moreover, we examined the involvement of MEK-ERK signaling in the effects of TNF on DA uptake. TNF-α increased DA uptake via the MEK-ERK signaling pathway in PC12 cells (Figs 1 and 2). The increase was antagonized by the anti-TNF-α antibody and soluble TNF receptor I (Fig. 1b and c), suggesting that TNF-α certainly increases DA uptake in PC12 cells. Moreover, TNF-α inhibited the METH-induced decrease in DA uptake in PC12 cells (Fig. 3b). We have previously reported that the kinetics of [^{3}H] DA uptake in the absence or presence of TNF-α (10 ng/mL). Lineweaver-burk plots show that TNF-α potentiates [^{3}H] DA uptake by increasing the affinity (Km) accompanied by reducing the maximum number of [^{3}H] DATs (Vmax) (Nakajima *et al.* 2004). We suggest that TNF-α modulates the function of DAT, although it also regulates the expression of DAT. The expression of TNF-α is induced through the activation of transcription factors such as activator protein-1 (AP-1) and NF-κB by the activation of JNK/p38 (Guha *et al.* 2000; Rahman and MacNee 2000). Further, TNF-α acts on mitochondria to generate reactive oxygen species, which are involved in the activation of AP-1 and NF-κB (Rahman and MacNee 2000). Changes in transcription factors may result in long-term changes in gene expression, thereby contributing to neuronal adaptations that underlie behavioral sensitization (Nestler 2001). Therefore, we hypothesized that TNF-α inhibits the METH-induced increase in extracellular DA levels in the NAc by promoting DA uptake and finally inhibits METH-induced sensitization and rewarding effects (Nakajima *et al.* 2004; Niwa *et al.* 2007c,e).

'Shati', named after the symbol for Nagoya castle, was identified among molecules whose expression was regulated in the NAc of mice treated with METH (Niwa *et al.* 2007a). Recently, we have demonstrated that blockage of shati expression by shati-AS potentiates the increase in extracellular DA levels in the NAc and the decrease in synaptosomal and vesicular DA uptake in the midbrain induced by repeated METH treatment (Niwa *et al.* 2007a). Both TNF-α and shati increase DA uptake and inhibit the METH-induced decrease in DA uptake (Nakajima *et al.* 2004; Niwa *et al.* 2007a). Therefore, we investigated the precise mechanism of the effects of shati on DA uptake, and the METH-induced inhibition of DA uptake in PC12 cells. Moreover, we examined the relationship between shati and TNF-α in PC12 cells. Over-expression of shati by transfection of the vector containing shati cDNA (Fig. 4) dramatically induced the expression of shati mRNA (Fig. 5a) and TNF-α mRNA (Fig. 6a) in PC12 cells. No histological or mechanical disruption was produced by transfection of the vector (Fig. 4a). Over-expression of shati (Fig. 5a), which occurs in TNF-α-immunopositive cells (Fig. 6d), potentiated DA uptake and inhibited the METH-induced decrease in DA uptake (Fig. 5b) in PC12 cells by regulating TNF-α expression (Fig. 6a), since these effects were antagonized by anti-TNF-α antibody and soluble TNF receptor I used for the neutralization of TNF-α (Fig. 6c; Barone *et al.* 1997). These findings strongly suggest that the over-expression of shati elicited by METH serves as a homeostatic mechanism that prevents behavioral sensitization and rewarding effects by attenuating the METH-induced increase in extracellular DA

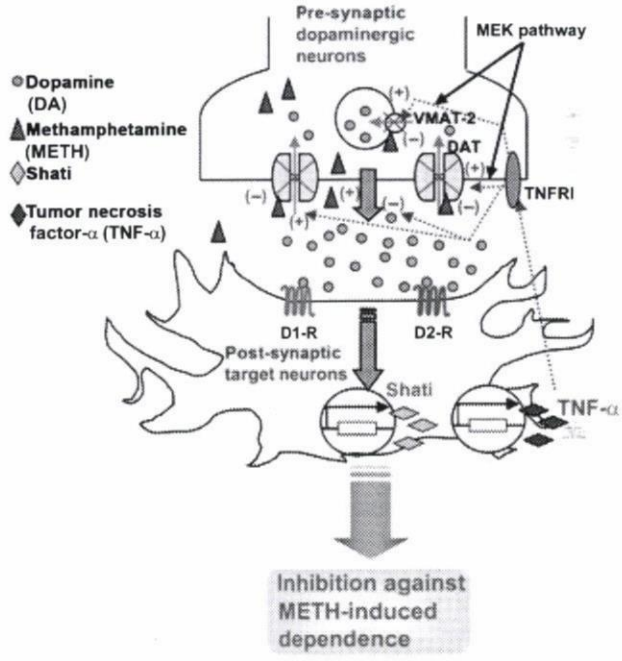

Fig. 7 Schema for regulation of TNF-α induced by shati on METH-induced DA responses. Under basal conditions, plasmalemmal DAT is involved in the reuptake of extracellular DA into the cytosol; subsequently the cytosolic DA is stored into synaptic vesicles via VMAT-2. Treatment of METH inhibits DA uptake through DA transporter and facilitates DA's release from pre-synaptic nerve terminals. METH is associated with an increase in extracellular DA levels in the brain, resulting in potentiation of the METH-induced dependence. METH induces shati and TNF-α expression in target neurons through the activation of DA receptors. TNF-α regulated by shati inhibits the METH-induced increase in extracellular DA levels in the nucleus accumbens by promoting DA uptake via MEK pathway and finally inhibits sensitization to and the rewarding effects of METH. DA: dopamine, METH: methamphetamine, TNF-α: tumor necrosis factor-α, D1-R: dopamine D1 receptor, D2-R: dopamine D2 receptor, DAT: dopamine transporter, VMAT-2: vesicular monoamine transporter-2, TNFR I: tumor necrosis factor type I receptor.

levels in the NAc through potentiation of plasmalemmal and vesicular DA uptake *via* induction of TNF-α expression (Fig. 7), although the mechanism by which TNF-α is regulated by shati remains to be elucidated.

Motif analyses have revealed that shati contains sequences of GNAT (Niwa *et al.* 2007a). Docking simulations with acetyl-CoA or ATP conducted using Molecular Operating Environment software reveal possible acetyl-CoA- and/or ATP-binding sites, since there is low potential energy for these interactions, in contrast with the prohibitively high energy of docking with DA, DNA or nuclear localization signals (Niwa *et al.* 2007a). These results suggest shati to have a physiological role in producing acetylcholine or the metabolic action of ATP. Accordingly, we have to investigate the mechanism by which shati regulates the production of acetylcholine or metabolic roles of ATP in subsequent studies.

In conclusion, we hypothesized that TNF-α expression induced by shati inhibits the METH-induced increase in extracellular DA levels in the NAc by promoting DA uptake and finally inhibits sensitization to and the rewarding effects of METH (Fig. 7). Targeting the shati-TNF-α system would provide a new therapeutic approach to the treatment of METH dependence.

Acknowledgments

This study was supported in part by Research Fellowships of the Japan Society for the Promotion of Science (JSPS) for Young Scientists; by Grants-in-aid for Scientific Research (B) and for Exploratory Research from the JSPS; by the 'Academic Frontier' Project for Private Universities (2007–2011) from the Ministry of Education, Culture, Sports, Science and Technology of Japan; by the International Research Project supported by the Meijo Asian Research Center (MARC); by Health and Labour Sciences Research on Regulatory Science of Pharmaceuticals and Medical Devices from the Ministry of Health, Labour and Welfare, Japan; by Research on Risk of Chemical Substances, Health and Labour Science Research Grants supported by the Ministry of Health, Labour and Welfare; by the Japan France Joint Health Research Program; and by the Uehara Foundation.

The authors are grateful to the Riken Cell Bank for the pheochromocytoma-12 (PC12) cells, and to Mrs. Nobuyoshi Hamada and Yoshiyuki Nakamura, Radioisotope Center Medical Branch, Nagoya University Graduate School of Medicine, for technical assistance.

References

Amara S. G. and Kuhar M. J. (1993) Neurotransmitter transporters: recent progress. *Annu. Rev. Neurosci.* **16**, 73–93.

Barone F. C., Arvin B., White R. F., Miller A., Webb C. L., Willette R. N., Lysko P. G. and Feuerstein G. Z. (1997) TNF-α. A mediator of focal ischemic brain injury. *Storoke* **28**, 1233–1244.

Baud V. and Karin K. (2001) Signal transduction by tumor necrosis factor and its relatives. *Trends Cell Biol.* **11**, 372–377. Review.

Boka G., Anglade P., Wallach D., Javoy-Agid F., Agid Y. and Hirsch E. C. (1994) Immunocytochemical analysis of tumor necrosis factor and its receptors in Parkinson's disease. *Neurosci. Lett.* **172**, 151–154.

Cen X., Nitta A., Ibi D., Zhao Y., Niwa M., Taguchi K., Hamada M., Ito Y., Ito Y., Wang L. and Nabeshima T. (2008) Identification of piccolo as a regulator of behavioral plasticity and dopamine transporter internalization. *Mol. Psychiatr.* **13**, 451–463.

Chen N. H., Reith M. E. and Quick M. W. (2004) Synaptic uptake and beyond: the sodium- and chloride-dependent neurotransmitter transporter family SLC6. *Pflugers Arch.* **447**, 519–531. Review.

Devin A., Lin Y. and Liu Z. G. (2003) The role of the death-domain kinase RIP in tumour-necrosis-factor-induced activation of mitogen-activated protein kinases. *EMBO* **4**, 623–627.

Finberg J. P. and Youdim M. B. (1983) Selective MAO A and B inhibitors: their mechanism of action and pharmacology. *Neuropharmacology* **22**, 441–446. Review.

Fog J. U., Khoshbouei H., Holy M. *et al.* (2006) Calmodulin kinase II interacts with the dopamine transporter C terminus to regulate amphetamine-induced reverse transport. *Neuron* **51**, 417–429.

Fornai F., Lenzi P., Lazzeri G., Ferrucci M., Fulceri F., Giorgi F. S., Falleni A., Ruggieri S. and Paparelli A. (2007) Fine ultrastructure and biochemistry of PC12 cells: a comparative approach to understand neurotoxicity. *Brain Res.* **1129**, 174–190.

Franklin K. B. J. and Paxinos G. (1997) *The Mouse Brain: In Stereotaxic Coordinates*. Academic Press, San Diego.

Grace A. A. (1995) The tonic/phasic model of dopamine system regulation: its relevance for understanding how stimulant abuse can alter basal ganglia function. *Drug Alcohol Depend.* **37**, 111–129. Review.

Greene L. A. and Rein G. (1978) Short-term regulation of catecholamine biosynthesis in a nerve growth factor responsive clonal line of rat pheochromocytoma cells. *J. Neurochem.* **30**, 549–555.

Guha M., Bai W., Nadler J. L. and Natarajan R. (2000) Molecular mechanisms of tumor necrosis factor α gene expression in monocytic cells via hyperglycemia-induced oxidant stress-dependent and -independent pathways. *J. Biol. Chem.* **275**, 17728–17739.

Horn A. S. (1990) Dopamine uptake: a review of progress in the last decade. *Prog. Neurobiol.* **34**, 387–400. review.

Hsu H., Xiong J. and Goeddel D. V. (1995) The TNF receptor 1-associated protein TRADD signals cell death and NF-kappa B activation. *Cell* **81**, 495–504.

Hyman S. E. (1996) Addiction to cocaine and amphetamine. *Neuron* **16**, 901–904.

Jones S. R., Gainetdinov R. R., Jaber M., Giros B., Wightman R. M. and Caron M. G. (1998) Profound neuronal plasticity in response to inactivation of the dopamine transporter. *Proc. Natl Acad. Sci. USA* **95**, 4029–4034.

Koob G. F. (1992) Drugs of abuse: anatomy, pharmacology and function of reward pathways. *Trends Pharmacol. Sci.* **13**, 177–184.

Koob G. F., Sanna P. P. and Bloom F. E. (1998) Neuroscience of addiction. *Neuron* **21**, 467–476.

Loder M. K. and Melikian H. E. (2003) The dopamine transporter constitutively internalizes and recycles in a protein kinase C-regulated manner in stably transfected PC12 cell lines. *J. Biol. Chem.* **278**, 22168–22174.

Maier S. F. and Watkins L. R. (1998) Cytokines for psychologists: implications of bidirectional immune-to-brain communication for understanding behavior, mood, and cognition. *Psychol. Rev.* **105**, 83–107.

Markey K. A., Kondo H., Shenkman L. and Goldstein M. (1980) Purification and characterization of tyrosine hydroxylase from a clonal pheochromocytoma cell line. *Mol. Pharmacol.* **17**, 79–85.

Melikian H. E. and Buckley K. M. (1999) Membrane trafficking regulates the activity of the human dopamine transporter. *J. Neurosci.* **19**, 7699–7710.

Morón J. A., Zakharova I., Ferrer J. V. *et al.* (2003) Mitogen-activated protein kinase regulates dopamine transporter surface expression and dopamine transport capacity. *J. Neurosci.* **23**, 8480–8488.

Nakajima A., Yamada K., Nagai T. *et al.* (2004) Role of tumor necrosis factor-α in methamphetamine-induced drug dependence and neurotoxicity. *J. Neurosci.* **24**, 2212–2225.

Nestler E. J. (2001) Molecular basis of long-term plasticity underlying addiction. *Nat. Rev. Neurosci.* **2**, 119–128.

Niwa M., Nitta A., Mizoguchi H., Ito Y., Noda Y., Nagai T. and Nabeshima T. (2007a) A novel molecule 'shati' is involved in methamphetamine-induced hyperlocomotion, sensitization, and conditioned place preference. *J. Neurosci.* **27**, 7604–7615.

Niwa M., Nitta A., Shen L., Noda Y. and Nabeshima T. (2007b) Involvement of glial cell line-derived neurotrophic factor in inhibitory effects of a hydrophobic dipeptide Leu-Ile on morphine-induced sensitization and rewarding effects. *Behav. Brain Res.* **179**, 167–171.

Niwa M., Nitta A., Yamada K. and Nabeshima T. (2007c) The roles of glial cell line-derived neurotrophic factor, tumor necrosis factor-α, and an inducer of these factors in drug dependence. *J. Pharmacol. Sci.* **104**, 116–121.

Niwa M., Nitta A., Yamada Y., Nakajima A., Saito K., Seishima M., Noda Y. and Nabeshima T. (2007d) Tumor necrosis factor-α and its inducer inhibit morphine-induced rewarding effects and sensitization. *Biol. Psychiatry* **62**, 658–668.

Niwa M., Nitta A., Yamada Y., Nakajima A., Saito K., Seishima M., Shen L., Noda Y., Furukawa S. and Nabeshima T. (2007e) An inducer for glial cell line-derived neurotrophic factor and tumor necrosis factor-α protects against methamphetamine-induced rewarding effects and sensitization. *Biol. Psychiatry* **61**, 890–901.

Niwa M., Yan Y. and Nabeshima T. (2008) Genes and molecules that can potentiate or attenuate psychostimulant dependence: relevance of data from animal models to human addiction. *Ann. NY Acad. Sci.* **1141**, 76–95.

Rahman I. and MacNee W. (2000) Regulation of redox glutathione levels and gene transcription in lung inflammation: therapeutic approaches. *Free Radic. Biol. Med.* **28**, 1405–1420.

Rawson R. A., Gonzales R. and Brethen P. (2002) Treatment of methamphetamine use disorders: an update. *J. Subst. Abuse Treat.* **23**, 145–150. Review.

Roda L. G., Nolan J. A., Kim S. U. and Hogue-Angeletti R. A. (1980) Isolation and characterization of chromaffin granules from a pheochromocytoma (PC 12) cell line. *Exp. Cell Res.* **128**, 103–109.

Sampath D., Jackson G. R., Werrbach-Perez K. and Perez-Polo J. R. (1994) Effects of nerve growth factor on glutathione peroxidase and catalase in PC12 cells. *J. Neurochem.* **62**, 2476–2479.

Self D. W. and Nestler E. J. (1995) Molecular mechanisms of drug reinforcement and addiction. *Annu. Rev. Neurosci.* **18**, 463–495. Review.

Sulzer D., Sonders M. S., Poulsen N. W. and Galli A. (2005) Mechanisms of neurotransmitter release by amphetamines: a review. *Prog. Neurobiol.* **75**, 406–433.

Tischler A. S. (2002) Chromaffin cells as models of endocrine cells and neurons. *Ann. NY Acad. Sci.* **971**, 366–370. Review.

Torres G. E., Gainetdinov R. R. and Caron M. G. (2003) Plasma membrane monoamine transporters: structure, regulation and function. *Nat. Rev. Neurosci.* **4**, 13–25. Review.

Vaccaro K. K., Liang B. T., Perelle B. A. and Perlman R. L. (1980) Tyrosine 3-monooxygenase regulates catecholamine synthesis in pheochromocytoma cells. *J. Biol. Chem.* **255**, 6539–6541.

Vassalli P. (1992) The pathophysiology of tumor necrosis factors. *Annu. Rev. Immunol.* **10**, 411–452. Review.

van Vliet C., Bukczynska P. E., Puryer M. A., Sadek C. M., Shields B. J., Tremblay M. L. and Tiganis T. (2005) Selective regulation of tumor necrosis factor-induced Erk signaling by Src family kinases and the T cell protein tyrosine phosphatase. *Nat. Immunol.* **6**, 253–260.

Wada R., Tifft C. J. and Proia R. L. (2000) Microglial activation precedes acute neurodegeneration in Sandhoff disease and is suppressed by bone marrow transplantation. *Proc. Natl Acad. Sci. USA* **97**, 10954–10959.

Wise R. A. (1996) Neurobiology of addiction. *Curr. Opin. Neurobiol.* **6**, 243–251.

Youdim M. B. (1991) PC12 cells as a window for the differentiation of neural crest into adrenergic nerve ending and adrenal medulla. *J. Neural Transm. Suppl.* **34**, 61–67.

0022-3565/08/3271-137–147$20.00
THE JOURNAL OF PHARMACOLOGY AND EXPERIMENTAL THERAPEUTICS
Copyright © 2008 by The American Society for Pharmacology and Experimental Therapeutics
JPET 327:137–147, 2008

Vol. 327, No. 1
141309/3384925
Printed in U.S.A.

The Extensive Nitration of Neurofilament Light Chain in the Hippocampus Is Associated with the Cognitive Impairment Induced by Amyloid β in Mice

Tursun Alkam, Atsumi Nitta, Hiroyuki Mizoguchi, Akio Itoh, Rina Murai, Taku Nagai, Kiyofumi Yamada, and Toshitaka Nabeshima

Department of Neuropsychopharmacology and Hospital Pharmacy, Nagoya University Graduate School of Medicine, Nagoya, Japan (T.A., A.N., H.M., A.I., R.M., T.Nag., K.Y., T.Nab.); Department of Basic Medicine, College of Traditional Uighur Medicine, Hotan, China (T.A.); and Department of Chemical Pharmacology, Graduate School of Pharmaceutical Science, Meijo University, Nagoya, Japan (T.Nab.)

Received May 19, 2008; accepted July 9, 2008

ABSTRACT

Tyrosine nitration of proteins at an extensive level is widely associated with the cognitive pathology induced by amyloid β peptide (Aβ). However, the precise identity and explicit consequences of protein nitration have scarcely been addressed. In this study, we examined the detectable nitration of proteins in the hippocampus of mice with cognitive impairment (day 5) induced by the i.c.v. injection of $A\beta_{25-35}$ (day 0). The intensity of the nitration of proteins was inversely associated with the level of recognition memory in mice. The detectable tyrosine nitrations were revealed in proteins with a single size of approximately 70 kDa. The specific nitrated proteins at this size were identified using the liquid chromatography/mass spectrometry/mass spectrometry analysis and immunodetection methods. Intense nitration of the neurofilament light chain (NFL) was observed. The increased nitration of NFL was associated with its serine hyperphosphorylation and weak interaction with the nuclear distribution element-like, a protein essential for the stable assembly of neurofilaments. No changes in cell numbers in the hippocampus were found (day 5) in mice that received $A\beta_{25-35}$ injections. These findings suggested that extensive nitration of NFL is associated with the Aβ-induced impairment of recognition memory in mice.

Increased nitration of proteins, a surrogate marker of widespread oxidative damage in brains affected by the amyloid β peptide (Aβ), is evidently correlated with the severity of cognitive dysfunction in humans as well as animals (Smith et al., 1997; Lim at al., 2001; Perry et al., 2002; Kim et al., 2003; Andersen, 2004; Bastianetto and Quirion, 2004; Walsh and Selkoe, 2004).

We have previously reported the contribution of tyrosine nitration to Aβ-induced, oxidative damage-mediated cognitive dysfunction in mice (Alkam et al., 2007, 2008). A mouse monoclonal anti-nitrotyrosine antibody in Western blot analysis identified the tyrosine-nitrated hippocampal proteins at approximately 70 kDa as a single band with which the severity of cognitive impairments in mice was well associated (Alkam et al., 2007). In this study, we aimed to identify the nitrated proteins in the single band for the specification of the contribution of the extensive nitration of tyrosine to the cognitive impairment. To produce strong and stable nitrative damage, we applied $A\beta_{25-35}$, a toxic Aβ fragment that is detected in the human brain (Pike et al., 1995; Kubo et al., 2002). The tyrosine-nitrated proteins were examined by using liquid chromatography/mass spectrometry/mass spec-

This work was supported, in part, by the following: Japan-China Sasakawa Medical fellowship (to T.A.); Uehara Memorial Foundation fellowship for Foreign Researchers in Japan (to T.A.); grant-in-aid for the 21st Century Center of Excellence Program "Integrated Molecular Medicine for Neuronal and Neoplastic Disorders" and "Academic Frontier Project for Private Universities (2007–2011)" from the Ministry of Education, Culture, Sports, Science and Technology of Japan; Comprehensive Research on Aging and Health from the Ministry of Health, Labor and Welfare of Japan; Japan-Canada Joint Health Research Program and Japan-France Joint Health Research Program (Joint Project from Japan Society for the Promotion of Science); and International Research Project Supported by the Meijo Asian Research Center.

Article, publication date, and citation information can be found at http://jpet.aspetjournals.org.

doi:10.1124/jpet.108.141309.

ABBREVIATIONS: Aβ, amyloid β peptide; LC-MS/MS, liquid chromatography/mass spectrometry/mass spectrometry; NFL, neurofilament light chain; NUDEL, nuclear distribution element-like; NF, neurofilament; $ONOO^-$, peroxynitrite; UA, uric acid; RIPA, radioimmunoprecipitation assay; PBS, phosphate-buffered saline; PAGE, polyacrylamide gel electrophoresis; PVDF, polyvinylidene difluoride; HSP70, heat shock protein 70; DRP-2, dihydropyrimidinase-like 2; GAPDH, glyceraldehyde 3-phosphate dehydrogenase; SD, sodium dithionite; CBB, Coomassie Brilliant Blue; AD, Alzheimer's disease.

trometry (LC-MS/MS) and immunodetection. Intense nitration of the neurofilament light chain (NFL) was observed. The intensive nitration was associated with serine hyperphosphorylation and reduced interaction of NFL with nuclear distribution element-like (NUDEL), a protein essential for the stable assembly of neurofilaments (NFs). The results provided further support for the conception that extensive nitration of tyrosine in proteins underlies one of the key mechanisms contributing to the cognitive pathology induced by Aβ.

Materials and Methods

Animals. Male ICR mice (Nihon SLC Co., Shizuoka, Japan) were used. The animals were housed in a controlled environment (23 ± 1°C, 50 ± 5% humidity) and allowed access to food and water ad libitum. The room lights were kept on between 8:00 AM and 8:00 PM. All experiments were performed in accordance with the Guidelines for Animal Experiments of Nagoya University Graduate School of Medicine. The procedures involving animals and their care conformed to the *Guidelines for Proper Conduct of Animal Experiments* (Science Council of Japan, 2006).

Treatment and Experimental Design. $A\beta_{25-35}$ (Bachem, Bubendorf, Switzerland) was dissolved in sterile double-distilled water to a stock concentration of 1 mg/ml and stored at −20°C before use. The dissolved $A\beta_{25-35}$ was incubated for aggregation at 37°C for 4 days. The distilled water was incubated at the same conditions and used as the vehicle. $A\beta_{1-40}$ (Bachem) was dissolved to a stock concentration of 1.0 mg/ml in 35% acetonitrile/0.1% trifluoroacetic acid and stored at −20°C before use. The solution of peroxynitrite ($ONOO^-$; 144 mM) (Millipore, Billerica, MA) was stored at −80°C before use. Incubated $A\beta_{25-35}$ (3 μg/3 μl), incubated distilled water (3 μl), $A\beta_{1-40}$ (5 μg/5 μl), and $ONOO^-$ (144 mM/1 μl) were administered by i.c.v. injection as described previously (Maurice et al., 1996; Alkam et al., 2007, 2008). In brief, a microsyringe with a 28-gauge stainless steel needle 3.0-mm long was used for all experiments. Mice were anesthetized lightly with ether, and the needle was inserted unilaterally 1 mm to the right of the midline point equidistant from each eye, at an equal distance between the eyes and the ears and perpendicular to the plane of the skull. A single shot of the indicated volume of agents was delivered gradually within 3 s. Mice exhibited normal behavior within 1 min after the injection. The injection placement or needle track was visible and was verified at the time of dissection. Neither insertion of the needle nor the volume of injection had a significant influence on survival, behavioral responses, or cognitive functions. Uric acid (UA) (Wako Pure Chemicals, Osaka, Japan) was prepared as a suspension in saline. Immediately after the single injection of $A\beta_{25-35}$ or $A\beta_{1-40}$, mice were given UA (100 mg/kg i.p.) daily for 6 consecutive days. The schedule of administration of peptides and drugs as well as biochemical, histochemical, and behavioral investigations is shown in Fig. 1.

Novel Object Recognition Task. This task, based on the spontaneous tendency of rodents to explore a novel object more often than a familiar one, was performed on days 3 to 5 after the i.c.v. injection of $A\beta_{1-40}$, $A\beta_{25-35}$, or peroxynitrite (day 0) as described previously (Alkam et al., 2007). A plastic chamber (35 × 35 × 35 cm) was used in low light conditions during the light phase of the light/dark cycle. The general procedure consisted of three different phases: 1) a habituation phase, 2) an acquisition phase, and 3) a retention phase. On the 1st day (habituation phase), mice were individually subjected to a single familiarization session of 10 min, during which time they were introduced into the empty arena to become familiar with the apparatus. On the 2nd day (acquisition phase), the animals were subjected to a single 10-min session, during which time two floor-fixed objects (A and B) were placed in a symmetric position from the center of the arena, 15 cm from each other and 8 cm from the nearest wall. The two objects, made of the same wooden material with a similar color and smell, were different in shape but identical in size. Mice were allowed to explore the objects in the open field. A preference index for each mouse was expressed as a ratio of the amount of time spent exploring object A (TA × 100)/(TA + TB), where TA and TB are the time spent exploring object A and object B, respectively. On the 3rd day (retention phase), mice were allowed to explore the open field in the presence of two objects: the familiar object A and a novel object C in different shapes but in similar color and size (A and C). A recognition index, calculated for each mouse, was expressed as the ratio (TC × 100)/(TA + TC), where TA and TC are the time spent during the retention phase on object A and object C, respectively. The time spent exploring the object (nose pointing toward the object at a distance ≤ 1 cm) was recorded by hand.

Sample Preparation. Animals were decapitated, and the hippocampi were removed on an ice-cold glass plate and stored at −80°C. Hippocampal protein extracts were obtained by homogenization in diverse ice-cold lysis buffers that included the radioimmunoprecipitation assay (RIPA) buffer, phosphate-buffered saline (PBS) buffer, Triton X-100 buffer, and 6 M urea buffer. The RIPA lysis buffer contained 20 mM trizma hydrochloride, pH 7.6, 150 mM sodium chloride, 2 mM EDTA·2Na, 50 mM sodium fluoride, 1 mM sodium vanadate, 1% Nonidet P-40, 1% sodium deoxycholate, 0.1% SDS, 1 mg/ml pepstatin, 1 mg/ml aprotinin, and 1 mg/ml leupeptin. The PBS lysis buffer, pH 7.4, contained 135 mM sodium chloride, 3.2 mM disodium hydrogen phosphate 12-water, 1.3 mM potassium chloride, and 0.5 mM potassium dihydrogen phosphate. The Triton X-100 buffer contained 10 mM trizma hydrochloride at pH 7.5, 150 mM sodium chloride, 1 mM EDTA at pH 8.0, and 1% Triton X-100. The 6 M urea lysis buffer contained 10 mM trizma base at pH 8.1, 6 M urea, and 1 mM dithiothreitol. All of these lysis buffers, with the exception of the RIPA buffer, were supplemented with complete protease inhibitor cocktail tablets (Roche Applied Science, Mannheim, Germany). Homogenates were centrifuged at 13000*g* for 20 min to obtain the desired supernatant of the extracts. The centrifuged pellets were washed twice with the previous buffer before being solubilized. The washing procedure consisted of complete dispersion of the pellets by vortexing and incubation in ice for 30 min followed by centrifugation at 13000*g* for 20 min. The unassembled NFL and NUDEL proteins were obtained within the soluble proteins in Triton X-100 buffer (Nguyen et al., 2004), and the insoluble protein pellets that include the assembled NFL and NUDEL proteins were then solubilized in 6 M urea lysis buffer (Crow et al., 1997). The cytoplasmic water-soluble proteins were obtained in PBS lysis buffer (Aoyama and Kitajima, 1999), and the insoluble pellets were then solubilized in Triton X-100 buffer. The concentrations of PBS-soluble and urea-soluble proteins were determined with a Bio-Rad protein assay reagent kit (Bio-Rad, Hercules, CA). The concentrations of the Triton

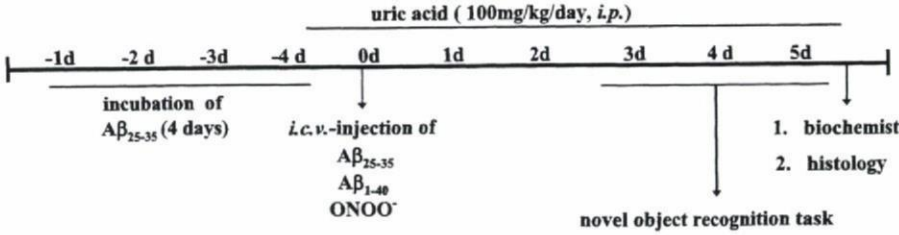

Fig. 1. The experimental design of the study.

X-100-soluble proteins were determined with a BCA protein assay reagent kit (Pierce, Rockford, IL).

Western Blot Analysis. Equal amounts (20 μg) of protein sample were resolved by a 4 to 20% gradient or 7% SDS-polyacrylamide gel electrophoresis (PAGE). The proteins were then transferred electrophoretically to a polyvinylidene difluoride (PVDF) membrane (Millipore). Membranes were incubated in 3% skim milk or 3% bovine serum albumin (for phosphor-protein) in phosphate-buffered saline containing 0.05% (v/v) Tween 20 for 2 h at room temperature. Anti-nitrotyrosine mouse monoclonal 1A6 antibody (catalog number 05-233; Millipore), anti-NFL mouse antibody (Sigma-Aldrich, St. Louis, MO), anti-heat shock protein 70 (HSP70) polyclonal antibody (Assay Designs, Ann Arbor, MI), anti-dihydropyrimidinase-like 2 (DRP-2) mouse antibody (IBL, Takasaki, Japan), anti-NUDEL rabbit antibody (Abcam Inc., Cambridge, MA), anti-phosphoserine rabbit antibody (Zymed Laboratories, South San Francisco, CA), anti-β-actin goat antibody (Santa Cruz Biotechnology Inc., Santa Crutz, CA), and anti-glyceraldehyde 3-phosphate dehydrogenase (GAPDH) mouse antibody (Imgenex, San Diego, CA) were used. To confirm the specificity of the detected single band of tyrosine-nitrated proteins, the reduction of nitrotyrosine to aminotyrosine was performed. In brief, the membrane was treated with 10 mM sodium dithionite (SD) in 50 mM pyridine-acetate buffer, pH 5.0, for 1 h at room temperature. After the reaction, the membrane was rinsed with distilled water and then equilibrated with washing buffer and blocked for 1 h at room temperature in blocking solution before standard procedures of Western blotting were followed. The absent band in the SD-treated membrane compared with the routine-treated control membrane was regarded to be a genuine for nitrated proteins. To confirm the specificity of the detected band for phosphoserine, the anti-phosphoserine inhibitor (the inhibitor) that contains phosphoserine was used to block the specific interaction of anti-phosphoserine primary antibodies with serine-phosphorylated proteins in the membrane. In brief, the anti-phosphoserine primary antibody and the inhibitor at a final concentration of 20 mM were mixed into a bovine serum albumin-containing blocking buffer and preincubated for 10 min for the ample binding of the antibodies with the phosphoserines (to cover up all of the specific anti-phosphoserine antibodies) before the application to the membrane. Incubation of the antibody-inhibitor mixture with the membrane was carried out for 1 h at room temperature. After the incubation, standard procedures were followed for blot washing and incubation with a secondary antibody. The absence of the bands in the membrane after the antibody-inhibitor treatment compared with the membrane subjected to routine treatment was regarded as genuine proof of serine phosphorylation. The intensity of each protein band on the film was analyzed with the Atto Densitograph 4.1 system (Atto, Tokyo, Japan) and was corrected with the corresponding β-actin or GAPDH level. The results were expressed as a percentage of that in the naive group.

Liquid Chromatography/Mass Spectrometry/Mass Spectrometry. Protein bands in the SDS-PAGE were stained with Coomassie Brilliant Blue (CBB) (Fluka, Buchs, Switzerland). The band of interest was excised from the gel. The gel piece was digested in trypsin solution at 35°C for 20 h for analysis by LC/MS/MS (Aproscience Lifescience Institute, Tokushima, Japan).

Immunoprecipitation. Hippocampal homogenates for Western blottings were used for immunoprecipitation. The antibodies against the proteins of interest were incubated overnight with 50 μl of protein A-Sepharose beads (GE Healthcare, Little Chalfont, Buckinghamshire, UK). To obtain tyrosine-nitrated proteins, anti-nitrotyrosine agarose-conjugated mouse antibody (Millipore) was used. The bead-antibody complexes were incubated overnight with 500 μg of precleared proteins in the corresponding buffers, with the exception that urea lysis buffer does not include dithiothreitol. Immunocomplexes were collected by centrifugation at 13000*g* for 1 min at 4°C and then washed three times with ice-cold PBS. Immunoprecipitated samples were recovered by resuspending in 2× sample loading buffer, immediately fractionated by reducing in 7% SDS-PAGE, and analyzed by Western blotting with the corresponding antibodies.

Histology. Each mouse was anesthetized with diethyl ether and quickly intracardially perfused with physiological saline followed by 4% paraformaldehyde in 100 mM PBS, pH 7.4. The brains were quickly removed, postfixed for 24 h in the same fixative solution, and cryoprotected in a graded 10 to 40% sucrose solution in 100 mM PBS. Coronal sections were cut 20-μm thick using a cryostat (Leica, Wetzlar, Germany) and stained with 0.1% cresyl violet reagent (Wako Pure Chemicals) according to standard procedures. The sections were mounted in fluorescent medium (Dako North America, Inc., Carpinteria, CA), and images of CA1, CA3, and the granular layer of the dentate gyrus of the hippocampus were taken using a Carl Zeiss Axioskop phase-contrast microscope with a cooled CCD camera system (SenSys; Photometrics Ltd., Tucson, AZ). The Nissl-positive neuronal cells were counted using Image J software (version 1.38; National Institutes of Health, Bethesda, MD). The total cell count in per millimeter square was averaged from four sections per animal ($n = 4$) according to previous reports (Nabeshima et al., 1991; Nitta et al., 1997).

Statistical Analysis. The results are expressed as the mean ± S.E. Statistical significance was determined with a one-way analysis of variance followed by the Bonferroni multiple comparisons test. $p < 0.05$ was taken as a significant level of difference.

Results

The Tyrosine Nitration of Proteins Induced by $A\beta_{25-35}$ in the Hippocampus of Mice. Anti-nitrotyrosine mouse antibody detected only a single band of hippocampal proteins at approximately 70 kDa for tyrosine nitration, which induced a potent nitrating agent after the i.c.v. injection of $A\beta_{1-40}$, $A\beta_{25-35}$, and peroxynitrite ($ONOO^-$) (Fig. 2A). Aβ peptides induced extensive nitration of proteins in the hippocampus and impairment of recognition memory, both of which were prevented by UA, a potent scavenger of $ONOO^-$. $ONOO^-$ induced marked tyrosine nitration of proteins in the hippocampus and impairment of recognition memory (Fig. 2, B and C). The intensity of the nitration was inversely associated with the recognition memory in mice (Fig. 2D). The authenticity of nitration was confirmed by the reduction of nitrotyrosine to aminotyrosine with SD in the membrane and by detecting the nitrotyrosine using the same antibody. The absence of this band after SD treatment was regarded as a genuine band for proteins with tyrosine nitration (Fig. 2, E and F). Proteins in SDS-PAGE were stained with CBB, and the 70-kDA protein band was excised for identification (Fig. 2G). The proteins in the excised gel were in-gel-trypsin-digested and subjected to LC/MS/MS, and several proteins were successfully identified (Table 1).

The Identification of the Tyrosine-Nitrated Proteins and the Level of Nitration. The nitration of the identified proteins was examined by applying the immunoprecipitation method. For peptide match scores, HSP70, DRP-2, and NFL were favored for the further study. Because the antibody that was used to detect the nitrated proteins in Western blot analysis could not be used for immunoprecipitation, a specially designed agarose-conjugated mouse anti-nitrotyrosine monoclonal antibody was used. We applied $A\beta_{25-35}$ for the rest of the study, considering its property to produce stronger and stable oxidative damage (Pike et al., 1995) as evidenced in Fig. 2. Immunoprecipitated nitrated-proteins were fractionated by SDS-PAGE and blotted with the antibodies raised against the proteins of interest (Fig. 3A). Intensive

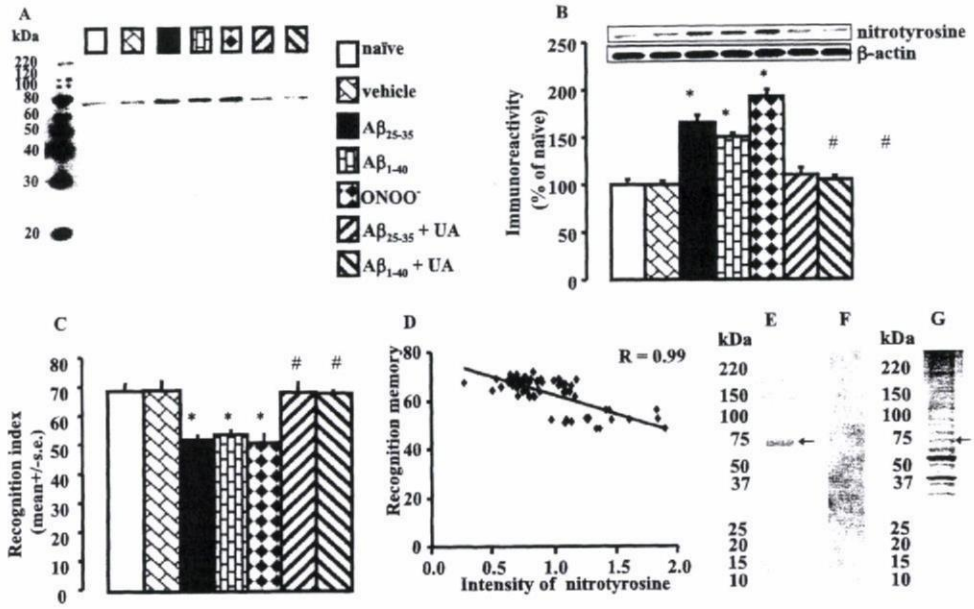

Fig. 2. The tyrosine nitration of proteins in the hippocampus and the cognitive function in mice. A and B, nitrotyrosine in the hippocampus was measured 5 days after the i.c.v. injection of Aβ peptides or $ONOO^-$. Protein samples from the hippocampus were subjected to SDS-PAGE, blotted to a PVDF membrane, and probed with a monoclonal anti-nitrotyrosine antibody. Aβ peptides induced extensive nitration of protein, which was prevented by UA, a potent scavenger of $ONOO^-$. $ONOO^-$ induced marked tyrosine nitration of proteins. The quantified intensity of the bands for nitrotyrosine was corrected by that of β-actin and expressed as a percentage of that in the naive group. Data are presented as the mean ± S.E. (n = 4). *, $p < 0.05$ versus naive and vehicle; #, $p < 0.05$ versus $A\beta_{25-35}$ or $A\beta_{1-40}$. C, the novel object recognition task was performed on days 3 to 5 after the i.c.v. injection of Aβ peptides or $ONOO^-$. Aβ peptides induced marked impairments of recognition memory, which were prevented by UA. $ONOO^-$ induced impairment of recognition memory. Data are presented as the mean ± S.E. (n = 10). *, $p < 0.05$ versus naive and vehicle; #, $p < 0.05$ versus $A\beta_{25-35}$ and $A\beta_{1-40}$. D, the panel shows the inverse association of extensive nitration of protein tyrosine in the hippocampus and the level of recognition memory in mice. E and F, protein samples from the hippocampus were subjected to 4 to 20% SDS-PAGE, blotted to PVDF membrane, and probed with a monoclonal anti-nitrotyrosine antibody before (E) and after (F) reduction of nitrotyrosine to aminotyrosine by treating the membrane with SD. G, protein bands in 4 to 20% SDS-PAGE were stained by CBB, and the band of interest was picked up for peptide analysis using LC-MS/MS.

TABLE 1
The identified protein candidates

Protein Name	gi Accession Number	Peptide Matched	% Sequence Coverage	Total Score
HSP70	gi 1661134	22	39	724
DRP-2	gi 40254595	7	20	292
NFL	gi 200038	4	9	254
ATPase, H^+transporting, V1 subunit A, isoform 1	gi 315607	9	17	184
Glycerol-3-phosphate dehydrogenase	gi 1339938	1	2	96
Ig superfamily receptor PGRL	gi 15593237	1	3	55
Solute carrier family 25 (mitochondrial carrier, aralar member12)	gi 27369581	3	8	53

gi, genInfo identifier; PGRL, prostaglandin regulatory-like protein.

nitration was observed for NFL in the $A\beta_{25-35}$ group compared with the naive or vehicle group (Fig. 3, A and B). No differences were observed in the nitration of HSP70 and DRP-2 proteins among the three groups (Fig. 3, A, C, and D). The increased nitration of NFL was inversely associated with recognition memory in mice that received $A\beta_{25-35}$ injections (Fig. 3E).

Association between Extensive Nitration of NFL and Serine Hyperphosphorylation. Hyperphosphorylation of the serine residues of NFL could lead to disruption of the subtle regulation of the NF network (Hisanaga et al., 1990; Nixon and Shea, 1992). After being nitrated in vitro, NFL is not able to form the NF assembly (Crow et al., 1997). The question of whether extensive nitration of NFL influences serine phosphorylation of the protein stimulated our interest. We immunoprecipitated NFL and blotted against nitrotyrosine and phosphoserine. Equal amounts of NFL protein were immunoprecipitated in each group (Fig. 4, A and B). The intensity of the tyrosine nitration and serine phosphorylation of NFL was greater in the $A\beta_{25-35}$ group than in the naive or vehicle group (Fig. 4, A, C, and D). The authenticity of the phosphoserine band was confirmed as indicated under *Materials and Methods*. Treatment with UA prevented the $A\beta_{25-35}$-induced intensive tyrosine nitration and serine hyperphosphorylation of NFL (Fig. 4, A, C, and D), indicating a positive association between the extensive nitration of NFL and the serine hyperphosphorylation (Fig. 4E).

Association between Extensive Nitration of NFL and Its Reduced Interaction with NUDEL. To examine whether the extensive nitration of NFL practically influences its interaction with partner proteins, we focused on the free, unassembled NFL that could be differentiated from the assembled NFL. The majority of the newly synthesized unassembled NF proteins, including NFL, are Triton X-100-solu-

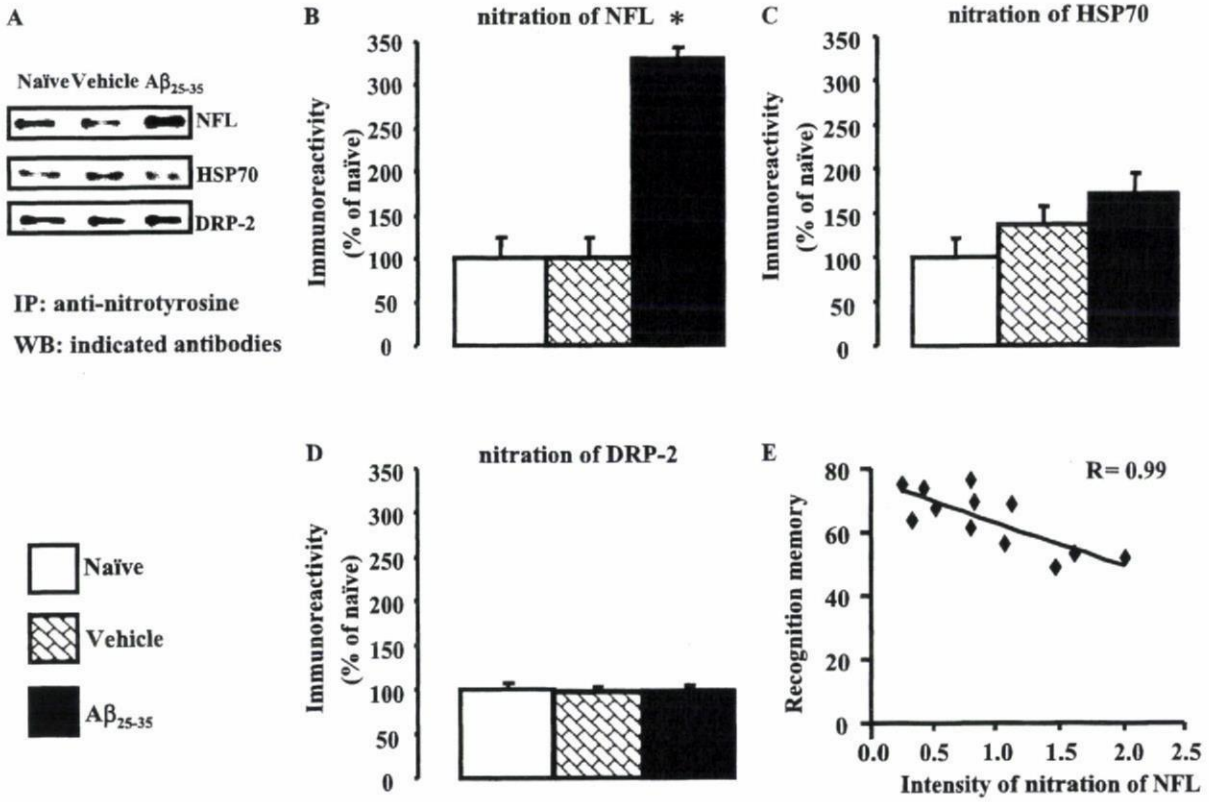

Fig. 3. Tyrosine nitration of the identified proteins. A, immunocomplexes, obtained from precleared protein samples of the hippocampus using an anti-nitrotyrosine agarose-conjugated mouse antibody, were separated by 7% SDS-PAGE, blotted onto a PVDF membrane, and probed with corresponding antibodies raised against the proteins of interest. B to D, NFL was intensely nitrated in the $A\beta_{25-35}$ group, whereas HSP70 and DRP-2 remained unchanged. E, the panel shows inverse association of the extensive nitration of NFL in the hippocampus (B) and the level of recognition memory in mice (Fig. 1B). The intensity of bands was quantified and expressed as a percentage of that in the naive group. Data are presented as the mean ± S.E. ($n = 4$). *, $p < 0.05$ versus naive and vehicle.

ble before being incorporated into the NF assembly, which is Triton X-100-insoluble (Black et al., 1986). NFL constitutes the core of the NF network, and without NFL, no filaments are formed (Zhu et al., 1997). Without binding directly with NUDEL, the Triton X-100-soluble NFL can barely lead the assembly of a stable NF network, regardless of its own abundance (Nguyen et al., 2004). We probed equal amounts of NFL immunocomplexes with antibodies raised against the nitrotyrosine and NUDEL (Fig. 5, A and B). Less NUDEL was coimmunoprecipitated in the $A\beta_{25-35}$ group that bears extensively nitrated NFL (Fig. 5, A–D). The protein expression of NUDEL did not differ among the groups (Fig. 5E). UA prevented the $A\beta_{25-35}$-induced increase of NFL nitration as well as the reduced coimmunoprecipitation of NUDEL (Fig. 5, A, C, and D). The extensive nitration of NFL was associated with its reduced interaction with NUDEL (Fig. 5F). These results suggested that the intensive nitration of NFL could disturb the normal function of the protein.

Association between Extensive Nitration of NFL and the Reduced Content of NUDEL in the Cytoskeleton Fraction. A majority of NF proteins, after their synthesis in the cytoplasm, are rapidly converted to a Triton X-100-insoluble filamentous network and move down the axon using the transport machinery (Nixon and Shea, 1992). After direct and specific binding with NFL, NUDEL facilitates the assembly of a stable NF network and remains bound to the assembled filaments (Nguyen et al., 2004). Thus, the level of interaction between NFL and NUDEL in cytoplasm (Triton X-100-soluble fraction) should be reflected by their protein levels in the axonal cytoskeleton (Triton X-100-insoluble fraction). The Triton X-100-insoluble fractions from the previous step (Fig. 5) were washed twice with Triton X-100 lysis buffer before being solubilized in urea lysis buffer. Western blot analysis revealed that the level of NUDEL protein was reduced in the $A\beta_{25-35}$ group compared with the naive and vehicle groups, whereas the treatment with UA prevented the reduction (Fig. 6, A and D). This was consistent with the reduced interaction between NFL and NUDEL in the $A\beta_{25-35}$ group (Fig. 5, A and D). However, the level of NFL in the $A\beta_{25-35}$ group was surprisingly not different from that in the naive and vehicle groups (Fig. 6, A and B). Considering the increase of the intensity of the protein nitration in the $A\beta_{25-35}$ group (Fig. 6, A and C), we examined the nitration of NFL by immunoprecipitation. Intense nitration for the NFL protein in the $A\beta_{25-35}$ group was observed (Fig. 6E). Applying the multiplicative inverse (in which the inverse or reciprocal of "n" is "1/n"), a mathematical method that is useful in medical science (Silberberg, 1990), the reciprocal level of the extensively nitrated NFL in the Triton X-100-insoluble fraction was estimated (Fig. 6F). The reciprocal level of extensively nitrated NFL in the $A\beta_{25-35}$ group paralleled with that of NUDEL in the same group (Fig. 6, D and F), signifying a negative effect of the extensive nitration of NFL on NUDEL-dependent NF assembly. The increased nitration of tyrosine could modify protein function by altering the three-dimensional conformation and hydrophobicity (Dalle-Donne et al.,

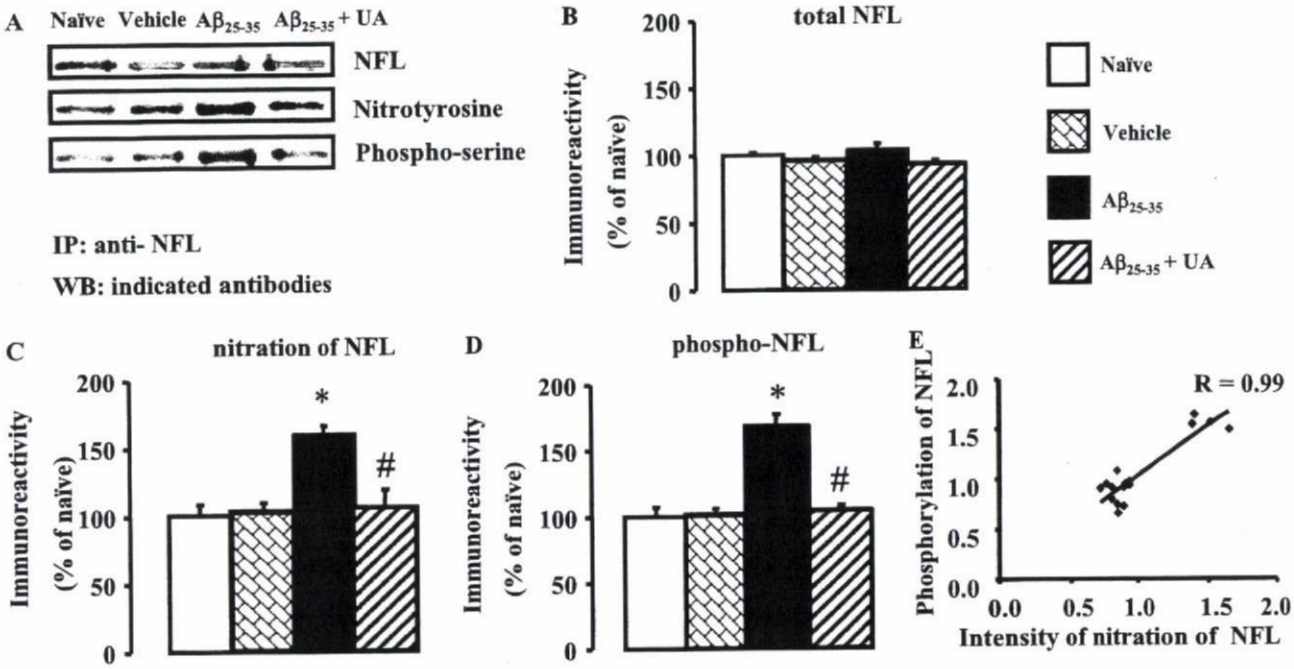

Fig. 4. The association between the increased tyrosine nitration and serine hyperphosphorylation of NFL. A, equal amounts of NFL protein immunocomplexes were obtained from precleared protein samples of the hippocampus, using anti-NFL antibody. The immunocomplexes were separated on SDS-PAGE, blotted onto a PVDF membrane, and probed with the indicated antibodies. B to D, tyrosine nitration and serine phosphorylation of NFL were increased in the $A\beta_{25-35}$ group, whereas UA prevented the increase of both. E, the increased nitration of NFL was correlated with serine hyperphosphorylation of NFL. The intensity of bands was quantified and expressed as a percentage of that in the naive group. Data are presented as the mean ± S.E. ($n = 4$). *, $p < 0.05$ versus naive and vehicle; #, $p < 0.05$ versus $A\beta_{25-35}$.

2005; Reynolds et al., 2007). It was therefore assumed that the overnitrated, free NFL would become less Triton X-100 soluble and, as a result, would be detected in the Triton X-100-insoluble fraction along with the assembled NF proteins. It is hardly practical to separate the unassembled extensively nitrated NFL from the assembled NFL in the Triton X-100-insoluble fraction. The majority of the cytoplasmic water-soluble proteins could be separated from the Triton X-100-soluble protein pools by using PBS lysis buffer in the first step (Aoyama and Kitajima, 1999). After the separation of the PBS-soluble and Triton X-100-soluble proteins as described under *Materials and Methods*, we examined the amount of NFL protein in these two different fractions. The majority of NFL protein in all groups was found in the PBS-soluble cytoplasmic fraction as indicated by GADPH, a cytoplasmic marker (Fig. 7A). The levels of NFL protein in both the PBS-soluble and Triton X-100-soluble fractions were increased in the $A\beta_{25-35}$ group (Fig. 7, A–C). It is interesting to note that the increase of NFL in both fractions was prevented by the treatment with of UA, a potent scavenger of $ONOO^-$, suggesting that the $A\beta_{25-35}$-induced $ONOO^-$ may increase the protein synthesis of NFL before extensively nitrating the protein (Fig. 7, A–C). The Triton X-100-soluble NFL that became insoluble in PBS in the $A\beta_{25-35}$ group was extensively nitrated (Fig. 7D), and the intensity of nitration was associated with the level of the PBS-insoluble, Triton X-100-soluble NFL (Fig. 7E). These results revealed new possibilities for Triton X-100-insolubile NFL in association with extensive nitration.

The Cell Numbers in the Hippocampus of Mice with the Impairment of Memory Induced by $A\beta_{25-35}$. On day 5 after the i.c.v. injection of $A\beta_{25-35}$, cell numbers in CA1, CA3, and the granular layer of the dentate gyrus of the hippocampal formation were examined using cresyl violet staining. The quantification of the stained cells revealed no cell loss induced by $A\beta_{25-35}$ (Table 2). These results were consistent with reports that at a dose of 3 to 5 μg, $A\beta_{25-35}$ could induce memory impairment but not cell loss within a time session of 1 month after its injection in mice (Maurice et al., 1996; Tohda et al., 2003). These results suggest that cell loss was not involved in the impairment of memory induced by $A\beta_{25-35}$ in mice.

Discussion

Neuronal oxidative damage has long been hypothesized as a critical mechanism of cellular dysfunction in neurodegenerative ailments (Perry et al., 2002). Reports showing that antioxidants delay or reduce progressive cognitive decline in both animal models and humans have emphasized the direct contribution of oxidative damage to cognitive pathology (Sano et al., 1997; Yamada et al., 1999; Lim et al., 2001). Oxidative damage is generally manifested by the increase of lipid peroxidation, DNA oxidation, protein oxidation, and peroxynitrite-mediated tyrosine nitration of proteins. The increased nitration of tyrosine could irreversibly disrupt the function of proteins (Koppal et al., 1999), and it might play a key pathogenic role in the progression of cognitive impairment (Smith et al., 1997; Keller, 2006). Until now, various proteins with tyrosine nitration have been reported in association with neurodegeneration and cognitive decline (Strong et al., 1998; Castegna et al., 2003; Tran et al., 2003; Sacksteder et al., 2006; Sultana et al., 2006). The diversity of nitrated proteins in these reports seems to depend on the species of the sources of samples (Sacksteder et al., 2006;

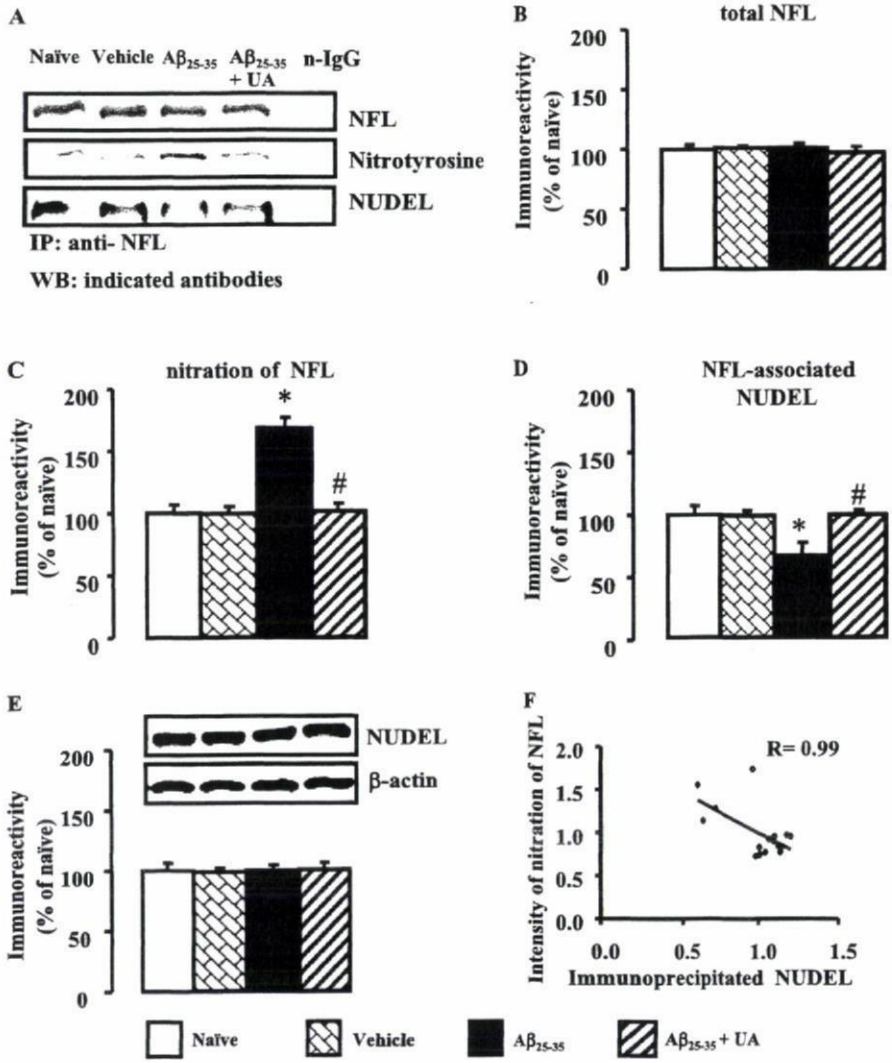

Fig. 5. Association between the extensive nitration of NFL and the reduced interaction with NUDEL in the Triton X-100-soluble fraction. A, the immunocomplexes obtained with the anti-NFL antibody, from precleared protein samples of the hippocampal homogenates, were separated by SDS-PAGE, blotted onto a PVDF membrane, and probed with the indicated antibodies. B, equal amounts of NFL protein were obtained. C, tyrosine nitration of NFL was increased in the $A\beta_{25-35}$ group, whereas UA treatment prevented the increase. D, the level of NFL-interacting NUDEL was reduced in the $A\beta_{25-35}$ group, whereas UA treatment prevented the reduction. E, no difference in NUDEL protein expression was found among the groups. F, the increased nitration of NFL was associated with reduced interaction with NUDEL. The intensity of bands was quantified and expressed as a percentage of that in the naive group. Data were presented as the mean ± S.E. ($n = 4$). *, $p < 0.05$ versus naive and vehicle; #, $p < 0.05$ versus $A\beta_{25-35}$.

Sultana et al., 2006), the proteomic detections on various conditions (Castegna et al., 2003; Sultana et al., 2006), immunodetections by means of different anti-nitrotyrosine antibodies with the diverse recognition property for nitrotyrosine (Strong et al., 1998; Tran et al., 2003), or the biological selectivity of tyrosine nitration (Ischiropoulos, 2003; Sacksteder et al., 2006). Dissimilar reports about the nitrated proteins in the brains of humans with Alzheimer's disease (AD) (Castegna et al., 2003; Sultana et al., 2006) emphasize the importance of the sources of protein, even in the same species or under the same conditions of detection during the identification process, while illustrating the diversity of nitration due to the dissimilar expression of proteins during the different stages of the disease.

In the present study, we looked for further evidence for the pathogenic role of protein nitration as one of the key contributors to the decline of cognitive function induced by Aβ. Using LC-MS/MS and immunodetection, we identified the hippocampal proteins with nitrated tyrosine residues after the i.c.v. injection of $A\beta_{25-35}$ in mice. Preferentially, in respect with currently examined proteins, intense nitration of NFL was observed, demonstrating a good correlation with the severity of cognitive impairment induced by $A\beta_{25-35}$.

NFL, one of the three subunits of NF proteins, is the indispensable core of the NF assembly (Zhu et al., 1997). Studies have reported that NFL is selectively nitrated compared with the majority of other proteins present in brain homogenates, and they suggested that newly synthesized free NFL is particularly susceptible to peroxynitrite-mediated nitration (Crow et al., 1997; Strong et al., 1998). The extensively nitrated NFL inhibits the assembly of unmodified NF subunits (Crow et al., 1997). On the other hand, the extensive serine phosphorylation of NFL could sufficiently block NF assembly (Nixon and Shea, 1992; Gibb et al., 1996). Therefore, we have evaluated the effect of tyrosine nitration on the phosphorylation of NFL at serine residues in general. The increased tyrosine nitration of NFL was associated with its serine hyperphosphorylation. Prevention of the extensive nitration of NFL by UA, a scavenger of $ONOO^-$ that nitrates proteins, restrained the serine phosphorylation of NFL at a normal level. The results indicated that the increased nitration of NFL could give rise to its serine hyperphosphorylation.

NFL requires direct binding with NUDEL, whereas NUDEL can not directly bind with other subunits of NF proteins, to initiate the assembly of NF (Nguyen et al., 2004). After the assembly of the NF network, NUDEL remains bound to the assembled Triton X-100-insoluble neurofilaments and may promote, in conjunction with molecular mo-

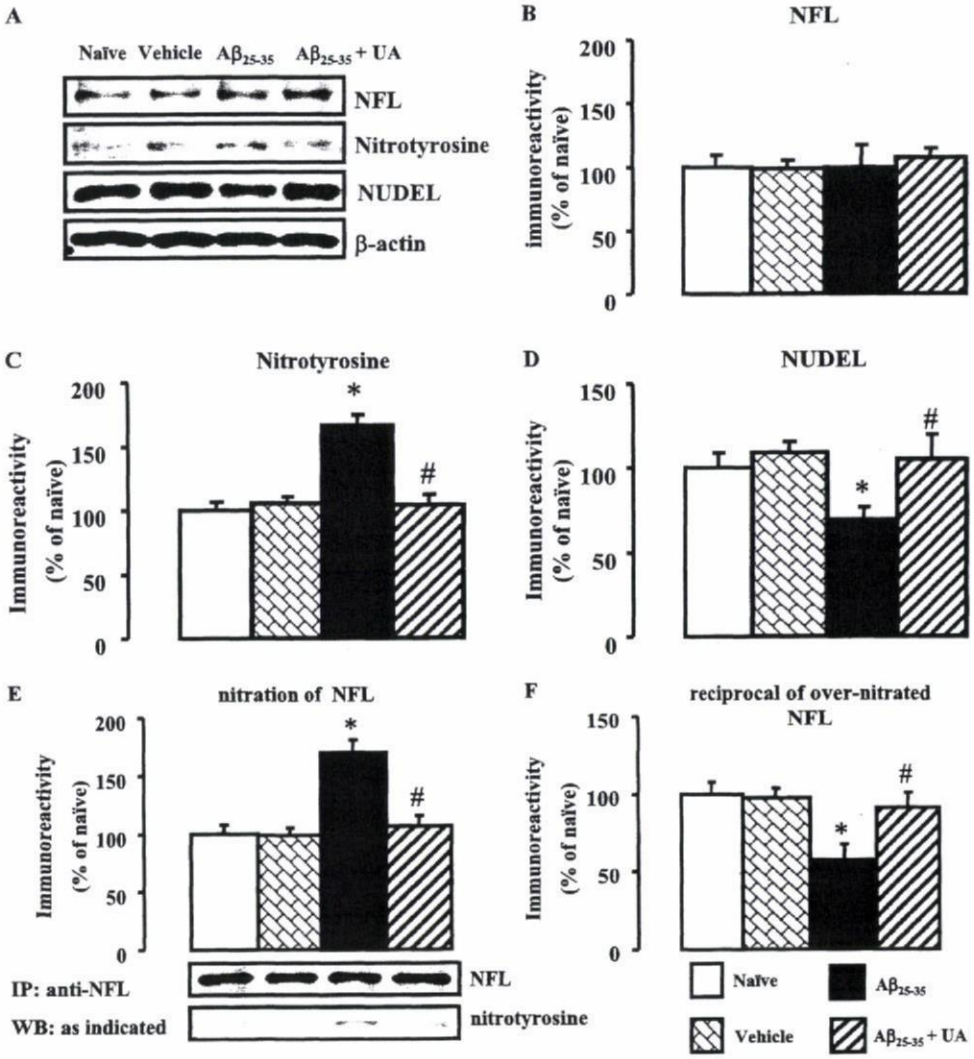

Fig. 6. The reduced content of NUDEL in the Triton X-100-insoluble cytoskeletal fraction. The Triton X-100-insoluble fraction, including cytoskeletal proteins, was solubilized in 6 M urea. A, equal amounts of protein were subjected to Western blot analysis. B, the protein levels of NFL were unchanged in all groups. C, the intensity of nitrotyrosine was increased in the $A\beta_{25-35}$ group, and the increase was prevented by UA, a scavenger of $ONOO^-$ that nitrates tyrosine. D, the protein level of NUDEL was reduced in the $A\beta_{25-35}$ group, and UA prevented this reduction. The quantified intensity of the bands was corrected by that of β-actin and expressed as a percentage of that in the naive group. E, equal amounts of NFL protein were immunoprecipitated and probed with anti-nitrotyrosine antibodies. The intensity of nitrotyrosine in NFL was increased in the $A\beta_{25-35}$ group, whereas UA prevented any increase. F, the reciprocal of the overnitrated NFL was estimated by applying multiplicative inverse (or reciprocal, in which the reciprocal of n is 1/n). The intensity of bands was quantified and expressed as a percentage of that in the naive group. Data are presented as the mean ± S.E. ($n = 4$). *, $p < 0.05$ versus naive and vehicle; #, $p < 0.05$ versus $A\beta_{25-35}$.

tors, the axonal transport of the neurofilaments (Nguyen et al., 2004). Thus, the level of interaction between NFL and NUDEL in the Triton X-100-soluble cytoplasmic fraction could be reflected by their protein levels in the Triton X-100-insoluble cytoskeletal fraction. In the current study, the increased nitration of Triton X-100-soluble NFL proteins in the $A\beta_{25-35}$ group was associated with its decreased interaction with NUDEL. In the Triton X-100-insoluble fraction, the protein level of NUDEL was reduced in the $A\beta_{25-35}$ group, and the reduction was prevented by treatment with UA. In the same fraction, the protein level of NFL surprisingly did not differ among groups, whereas the intensity of the nitration of NFL was strong in $A\beta_{25-35}$ group. Estimation by the multiplicative inverse approach indicated that the reduced level of nonextensively nitrated NFL in the $A\beta_{25-35}$ group parallels with that of NUDEL. These results required an explanation for the detection of the extensively nitrated NFL in the Triton X-100-insoluble cytoskeletal fraction, because the assembled NFL is nitration-resistant and the intensely nitrated NFL can not participate in the NF assembly (Crow et al., 1997). The alteration of the solubility of the overnitrated NFL might be involved in the detection of the extensively nitrated NFL in the Triton X-100-insoluble cytoskeletal fraction in the $A\beta_{25-35}$ group. Interpretation of the emergence of the intensely nitrated NFL in PBS-insoluble, but Triton X-100-soluble, protein pools in the $A\beta_{25-35}$ group indicates that extensive nitration would render NFL protein to have poor solubility in PBS. By this rate, it is possible that a considerable level of overnitrated NFL protein in the $A\beta_{25-35}$ group would even become Triton X-100 insoluble over a period of time, and that it would be detected along with a reduced level of NUDEL-associated assembled NFL, which is also Triton X-100 insoluble. The observation of detectable levels of nitration in NFL in the RIPA-soluble, Triton X-100-soluble, and Triton X-100-insoluble fractions in the naive and vehicle groups implies that natural nitration of tyrosine, as serine phosphorylation, might exist as a physiological property of NFL and might not be detrimental to the function of the protein, whereas extensive nitration is detrimental. The nitration-susceptible tyrosine residues of NFL are identified particularly as tyrosine 17 in the head region and tyrosines 138, 177, and 265 in the α-helical coil regions of the rod domain of the protein (Crow et al., 1997). It needs to be determined which tyrosine residue is the site for natural nitration or for extensive nitration. It has been reported that, although the exact mechanism is not clear, the newly synthesized Triton X-100-soluble NF proteins, including NFL, could separately undergo axonal transport before being in-

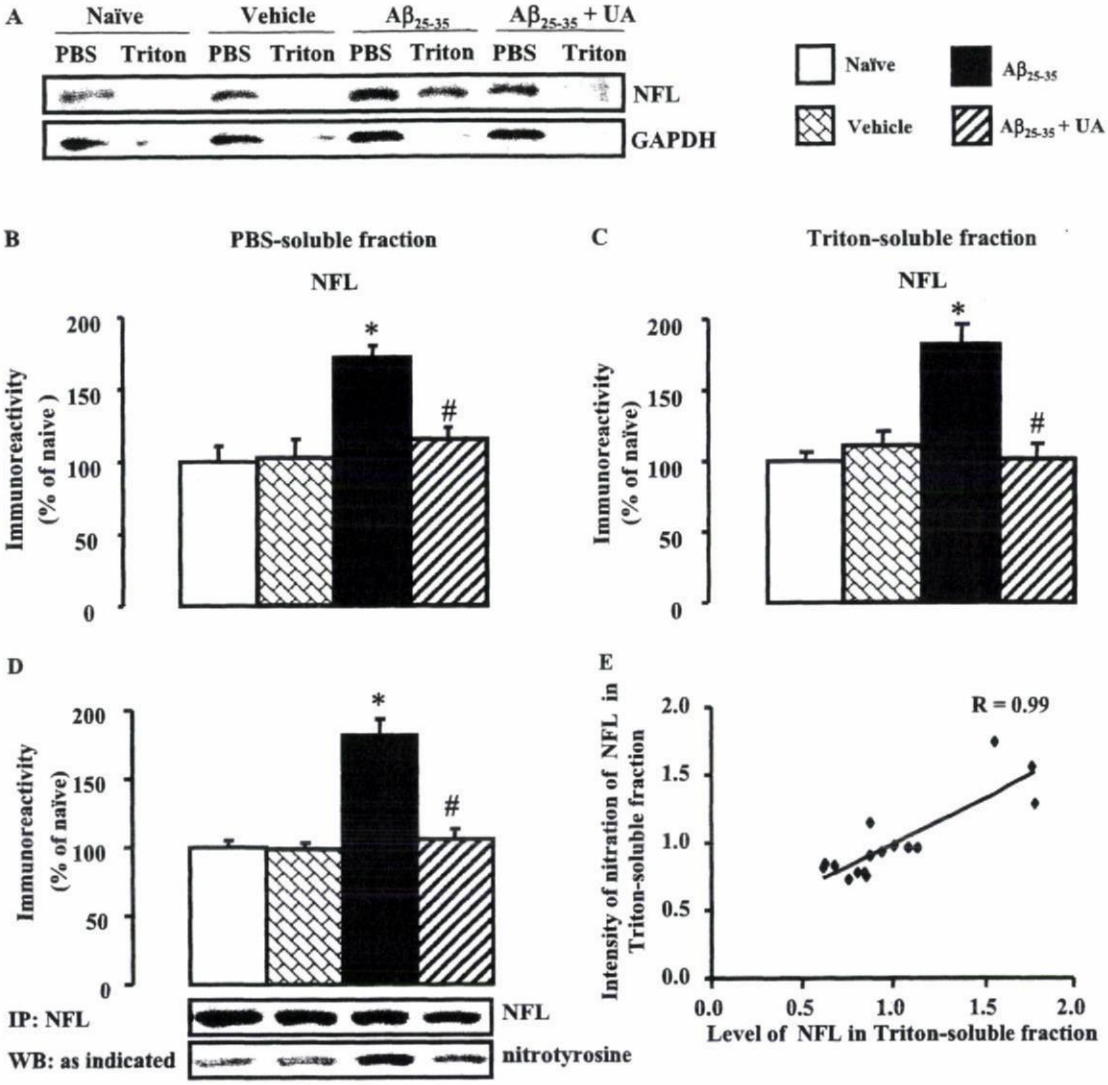

Fig. 7. The association of the extensive nitration of NFL with the alteration of solubility. The hippocampal tissues were homogenated in PBS and centrifuged at 13000*g* for 20 min, the washed pellets were solubilized in Triton X-100 as described under *Materials and Methods*, and equal amounts of protein were subjected to Western blot analysis. A to C, a majority of NFL and GAPDH proteins were soluble in PBS. NFL protein in the $A\beta_{25-35}$ group in both the PBS-soluble fraction and the Triton X-100-soluble fraction was increased, and the increase was prevented by UA, a scavenger of $ONOO^-$ that nitrates tyrosine. The quantified intensity of the bands was corrected by that of GAPDH and expressed as a percentage of that in the naive group. D, equal amounts of NFL from the Triton X-100-soluble proteins were immunoprecipitated and probed with anti-nitrotyrosine antibodies. The intensity of nitrotyrosine in NFL was increased in the $A\beta_{25-35}$ group, whereas UA prevented the increase. The intensity of bands was quantified and expressed as a percentage of that in the naive group. E, the level of NFL in the Triton X-100-soluble (PBS-insoluble) fraction was associated with the intensity of its nitration. Data are presented as the mean ± S.E. ($n = 4$). *, $p < 0.05$ versus naive and vehicle; #, $p < 0.05$ versus $A\beta_{25-35}$.

TABLE 2
The Nissl-positive cells in the hippocampus
In each group, $n = 4$.

Subfields of Hippocampus	Number of Nissl-Positive Cells			
	Naive	Vehicle	$A\beta_{25-35}$	$A\beta_{25-35}$ + UA
	counts/mm²			
CA1	10800 ± 230	10900 ± 290	10850 ± 250	10790 ± 270
CA3	6750 ± 190	6690 ± 210	6698 ± 180	6680 ± 310
GrDG	21000 ± 670	20980 ± 590	20990 ± 710	20780 ± 690

GrDG, the granular layer of the dentate gyrus.

corporated into the Triton X-100-insoluble axonal cytoskeleton (Jung et al., 1998). We do not know whether the NFL proteins with natural nitration undergo axonal transport after the NF assembly or undergo axonal transport before being incorporated into the Triton X-100-insoluble axonal cytoskeleton.

The observation of no cell loss in CA1, CA3, and the granular layer of the dentate gyrus of the hippocampus in mice

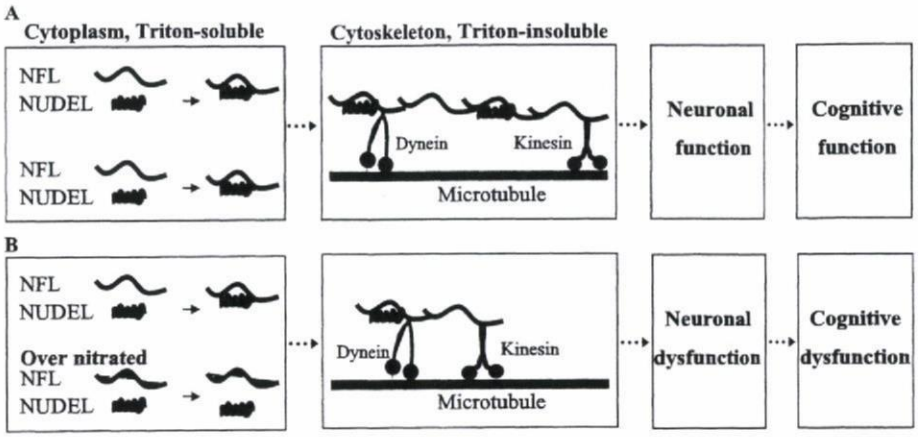

Fig. 8. The contribution of the extensive nitration of NFL to cognitive dysfunction. A, in this model, NFL interacts with NUDEL, which is essential for the incorporation of NF subunits into the network during NF assembly and elongation. A normal NF assembly and elongation favors normal neuronal and cognitive functions. B, the overnitration of NFL disrupts the interaction of NFL with NUDEL and may lead to the defective assembly of NF and abnormalities in neuronal and cognitive functions. The resized microtubules, kinesin, and dyenin have been added for clarity (modified from Nguyen et al., 2004; Holzbaur, 2004).

that received $A\beta_{25-35}$ injections favored the contribution of extensive nitration of NFL to the impairment of memory. A recent study demonstrated that rapidly formed fresh amyloid plaques cause axonal and dendritic structural changes within a minimum of 5 days after the "birth of the plaques" (Meyer-Luehmann et al., 2008). Given the time windows of Aβ neurotoxicity, $A\beta_{25-35}$ may require longer time to cause cell loss in our mouse model of cognitive impairment.

The disrupted interaction between NFL and NUDEL is regarded as the most important factor for the destabilization of the NF assembly that leads to the axonal dysfunction, which is an early event in the cognitive pathology of AD (Nguyen et al., 2004; Stokin et al., 2005). Therefore, our results suggest that disrupted interaction between NUDEL and NFL with extensive nitration could be one of the major factors that associated with the cognitive dysfunction induced by Aβ in mice (Fig. 8). However, further studies are required to investigate whether the extensive nitration of NFL and the impaired interaction with NUDEL induced by Aβ are associated with the disruption of axonal transport.

Acknowledgments

We are grateful to Dr. Minh Dang Nguyen for discussions on the sample preparation.

References

Alkam T, Nitta A, Mizoguchi H, Itoh A, and Nabeshima T (2007) A natural scavenger of peroxynitrites, rosmarinic acid, protects against impairment of memory induced by Aβ25–35. *Behav Brain Res* **180:**139–145.

Alkam T, Nitta A, Mizoguchi H, Saito K, Seshima M, Itoh A, Yamada K, and Nabeshima T (2008) Restraining tumor necrosis factor-alpha by thalidomide prevents the amyloid beta-induced impairment of recognition memory in mice. *Behav Brain Res* **189:**100–106.

Andersen JK (2004) Oxidative stress in neurodegeneration: cause or consequence? *Nat Med* **10:**S18–S25.

Aoyama Y and Kitajima Y (1999) Pemphigus vulgaris-IgG causes a rapid depletion of desmoglein 3 (Dsg3) from the Triton X-100 soluble pools, leading to the formation of Dsg3-depleted desmosomes in a human squamous carcinoma cell line, DJM-1 cells. *J Invest Dermatol* **112:**67–71.

Bastianetto S and Quirion R (2004) Natural antioxidants and neurodegenerative diseases. *Front Biosci* **9:**3447–3452.

Black MM, Keyser P, and Sobel E (1986) Interval between the synthesis and assembly of cytoskeletal proteins in cultured neurons. *J Neurosci* **6:**1004–1012.

Castegna A, Thongboonkerd V, Klein JB, Lynn B, Markesberyl WR, and Butterfield DA (2003) Proteomic identification of nitrated proteins in Alzheimer's disease brain. *J Neurochem* **85:**1394–1401.

Crow JP, Ye YZ, Strong M, Kirk M, Barnes S, and Beckman JS (1997) Superoxide dismutase catalyzes nitration of tyrosines by peroxynitrite in the rod and head domains of neurofilament-L. *J Neurochem* **69:**1945–1953.

Dalle-Donne A, Scaloni D, Giustarini E, Cavarra G, Tell G, Lungarella R, Colombo R, Rossi R, and Milzani A (2005) Proteins as biomarkers of oxidative/nitrosative stress in diseases: the contribution of redox proteomics. *Mass Spectrom Rev* **24:** 55–99.

Gibb BJ, Robertson J, and Miller CC (1996) Assembly properties of neurofilament light chain Ser55 mutants in transfected mammalian cells. *J Neurochem* **66:**1306–1311.

Hisanaga S, Gonda Y, Inagaki M, Ikai A, and Hirokawa N (1990) Effects of phosphorylation of the neurofilament L protein on filamentous structures. *Cell Regul* **1:**237–248.

Holzbaur EL (2004) Tangled NUDELs? *Nat Cell Biol* **6:**569–570.

Ischiropoulos H (2003) Biological selectivity and functional aspects of protein tyrosine nitration. *Biochem Biophys Res Commun* **305:**776–783.

Jung C, Yabe J, Wang FS, and Shea TB (1998) Neurofilament subunits can undergo axonal transport without incorporation into Triton-insoluble structures. *Cell Motil Cytoskeleton* **40:**44–58.

Keller JN (2006) Oxidative damage and oxidative stress in Alzheimer's disease. *Res Pract Alzheimer's Dis* **11:**110–114.

Kim HC, Yamada K, Nitta A, Olariu A, Tran MH, Mizuno M, Nakajima A, Nagai T, Kamei H, Jhoo WK, et al. (2003) Immunocytochemical evidence that amyloid beta (1–42) impairs endogenous antioxidant systems in vivo. *Neuroscience* **119:**399–419.

Koppal T, Drake J, Yatin S, Jordan B, Varadarajan S, Bettenhausen L, and Butterfield DA (1999) Peroxynitrite-induced alterations in synaptosomal membrane proteins: insight into oxidative stress in Alzheimer's disease. *J Neurochem* **72:**310–317.

Kubo T, Nishimura S, Kumagae Y, and Kaneko I (2002) In vivo conversion of racemized beta-amyloid ([D-Ser 26]A beta 1–40) to truncated and toxic fragments ([D-Ser 26]A beta 25–35/40) and fragment presence in the brains of Alzheimer's patients. *J Neurosci Res* **70:**474–483.

Lim GP, Chu T, Yang F, Beech W, Frautschy SA, and Cole GM (2001) The curry spice curcumin reduces oxidative damage and amyloid pathology in an Alzheimer transgenic mouse. *J Neurosci* **21:**8370–8377.

Maurice T, Lockhart BP, and Privat A (1996) Amnesia induced in mice by centrally administered beta-amyloid peptides involves cholinergic dysfunction. *Brain Res* **706:**181–193.

Meyer-Luehmann M, Spires-Jones TL, Prada C, Garcia-Alloza M, de Calignon A, Rozkalne A, Koenigsknecht-Talboo J, Holtzman DM, Bacskai BJ, and Hyman BT (2008) Rapid appearance and local toxicity of amyloid-beta plaques in a mouse model of Alzheimer's disease. *Nature* **451:**720–724.

Nabeshima T, Katoh A, Ishimaru H, Yoneda Y, Ogita K, Murase K, Ohtsuka H, Inari K, Fukuta T, and Kameyama T (1991) Carbon monoxide-induced delayed amnesia, delayed neuronal death and change in acetylcholine concentration in mice. *J Pharmacol Exp Ther* **256:**378–384.

Nguyen MD, Shu T, Sanada K, Larivière RC, Tseng HC, Park SK, Julien JP, and Tsai LH (2004) A NUDEL-dependent mechanism of neurofilament assembly regulates the integrity of CNS neurons. *Nat Cell Biol* **6:**595–608.

Nitta A, Fukuta T, Hasegawa T, and Nabeshima T (1997) Continuous infusion of beta-amyloid protein into the rat cerebral ventricle induces learning impairment and neuronal and morphological degeneration. *Jpn J Pharmacol* **73:**51–57.

Nixon RA and Shea TB (1992) Dynamics of neuronal intermediate filaments: a developmental perspective. *Cell Motil Cytoskeleton* **22:**81–91.

Perry G, Nunomura A, Hirai K, Zhu X, Pérez M, Avila J, Castellani RJ, Atwood CS, Aliev G, Sayre LM, et al. (2002) Is oxidative damage the fundamental pathogenic mechanism of Alzheimer's and other neurodegenerative diseases? *Free Rad Biol Med* **33:**1475–1479.

Pike CJ, Walencewicz-Wasserman AJ, Kosmoski J, Cribbs DH, Glabe CG, and Cotman CW (1995) Structure-activity analyses of Aβ peptides: contributions of the β25–35 region to aggregation and neurotoxicity. *J Neurochem* **64:**253–265.

Reynolds MR, Berry RW, and Binder LI (2007) Nitration in neurodegeneration: deciphering the "Hows" "nYs". *Biochemistry* **46:**7325–7336.

Sacksteder CA, Qian WJ, Knyushko TV, Wang H, Chin MH, Lacan G, Melega WP, Camp DG 2nd, Smith RD, Smith DJ, et al. (2006) Endogenously nitrated proteins in mouse brain: links to neurodegenerative disease. *Biochemistry* **45:**8009–8022.

Sano M, Ernesto C, Thomas RG, Klauber MR, Schafer K, Grundman M, Woodbury P, Growdon J, Cotman CW, Pfeiffer E, et al. (1997) A controlled trial of selegiline, alpha-tocopherol, or both as treatment for Alzheimer's disease. The Alzheimer's Disease Cooperative Study. *N Engl J Med* **336:**1216–1222.

Silberberg JS (1990) Estimating the benefits of cholesterol lowering: are risk factors for coronary heart disease multiplicative? *J Clin Epidemiol* **43:**875–879.

Smith MA, Richey Harris PL, Sayre LM, Beckman JS, and Perry G (1997) Wide-

spread peroxynitrite-mediated damage in Alzheimer's disease. *J Neurosci* **17:** 2653–2657.
Stokin GB, Lillo C, Falzone TL, Brusch RG, Rockenstein E, Mount SL, Raman R, Davies P, Masliah E, Williams DS, et al. (2005) Axonopathy and transport deficits early in the pathogenesis of Alzheimer's diseases. *Science* **307:**1282–1288.
Strong MJ, Sopper MM, Crow JP, Strong WL, and Beckman JS (1998) Nitration of the low molecular weight neurofilament is equivalent in sporadic amyotrophic lateral sclerosis and control cervical spinal cord. *Biochem Biophys Res Commun* **248:**157–164.
Sultana R, Poon HF, Cai J, Pierce WM, Merchant M, Klein JB, Markesbery WR, and Butterfield DA (2006) Identification of nitrated proteins in Alzheimer's disease brain using a redox proteomics approach. *Neurobiol Dis* **22:**76–87.
Tohda C, Tamura T, and Komatsu K (2003) Repair of amyloid beta (25–35)-induced memory impairment and synaptic loss by a Kampo formula, Zokumei-to. *Brain Res* **990:**141–147.
Tran MH, Yamada K, Nakajima A, Mizuno M, He J, Kamei H, and Nabeshima T (2003) Tyrosine nitration of a synaptic protein synaptophysin contributes to amyloid β-peptide-induced cholinergic dysfunction. *Mol Psychiatry* **8:**407–412.
Walsh DM and Selkoe DJ (2004) Deciphering the molecular basis of memory failure in Alzheimer's disease. *Neuron* **44:**181–193.
Yamada K, Tanaka T, Han D, Senzaki K, Kameyama T, and Nabeshima T (1999) Protective effects of idebenone and alpha-tocopherol on beta-amyloid-(1–42)-induced learning and memory deficits in rats: implication of oxidative stress in beta-amyloid-induced neurotoxicity in vivo. *Eur J Neurosci* **11:**83–90.
Zhu Q, Couillard-Després S, and Julien JP (1997) Delayed maturation of regenerating myelinated axons in mice lacking neurofilaments. *Exp Neurol* **148:**299–316.

Address correspondence to: Dr. Toshitaka Nabeshima, Department of Chemical Pharmacology, Graduate School of Pharmaceutical Science, Meijo University, Nagoya 468-8503, Japan. E-mail: tnabeshi@ccmfs.meijo-u.ac.jp

J Pharmacol Sci **108**, 408 – 414 (2008)

Journal of Pharmacological Sciences

Forum Minireview

Basic and Translational Research on Proteinase-Activated Receptors: Regulation of Nicotine Reward by the Tissue Plasminogen Activator (tPA) – Plasmin System via Proteinase-Activated Receptor 1

Taku Nagai[1], Toshitaka Nabeshima[2], and Kiyofumi Yamada[1,*]

[1]*Department of Neuropsychopharmacology and Hospital Pharmacy, Nagoya University Graduate School of Medicine, 65 Tsuruma-cho, Showa-ku, Nagoya 466-8560, Japan*
[2]*Department of Chemical Pharmacology, Graduate School of Pharmaceutical Sciences, Meijo University, Nagoya 468-8503, Japan*

Received July 3, 2008; Accepted September 24, 2008

Abstract. Nicotine, a primary component of tobacco, is one of the most abused drugs worldwide. Mesolimbic dopaminergic neurons mediate the rewarding effects of abused drugs, including nicotine. We show that the tissue plasminogen activator (tPA) – plasmin system regulates nicotine-induced reward and dopamine release in the nucleus accumbens (NAc) by activating proteinase-activated receptor 1 (PAR_1). Nicotine-induced conditioned place preference and dopamine release in the NAc are diminished in tPA knockout (tPA–/–) mice. The defect of nicotine-induced dopamine release in tPA–/– mice is reversed by microinjection of either exogenous tPA or plasmin into the NAc. Acute nicotine treatment increases tPA protein levels and promoted the release of tPA into the extracellular space. The expression of PAR_1 on dopaminergic neurons is evident and the activation of PAR_1 by plasmin is demonstrated by assaying GTP-γS binding. Finally, nicotine-induced conditioned place preference and dopamine release are diminished in PAR_1–/– mice. These findings suggest that targeting the tPA-plasmin–PAR_1 system would provide new therapeutic approaches for the treatment of nicotine dependence.

Keywords: dependence, dopamine, nicotine, proteinase-activated receptor 1 (PAR_1), tissue plasminogen activator (tPA)

Introduction

Tissue plasminogen activator (tPA), a serine protease that catalyzes the conversion of plasminogen (plg) to plasmin, plays an important role in fibrinolysis. This protease cascade is tightly regulated by the actions of serine protease inhibitors, of which plasminogen activator inhibitor-1 (PAI-1) and neuroserpin are the major cognate serpins for tPA, while plasmin is inhibited by α2-antiplasmin (1). Accumulating evidence has demonstrated that tPA is involved in synaptic plasticity and remodeling, directly by itself or indirectly through plasmin. For instance, tPA is directly involved in long-term potentiation (LTP) by acting on low-density lipoprotein receptor–related proteins (2) and NMDA receptors (3). On the other hand, neurite outgrowth (4), cell migration (5, 6), and amyloid-β degradation induced by tPA (7, 8) are mediated by plasmin. In addition, recent studies have demonstrated the role of tPA in the regulation of neurotransmitter release. Depolarization-evoked dopamine release in the NAc (9) as well as norepinephrine release from hearts (10) are diminished in tPA-deficient (tPA–/–) mice compared with wild-type mice. We have demonstrated that the tPA-plasmin system plays an important role in the rewarding effects of abused drugs, including methamphetamine and morphine (11 – 16).

Plasmin is known to degrade several extracellular matrix proteins, such as laminin (17), and converts pro-brain–derived neurotrophic factor to its mature form (18). Alternatively, plasmin was recently demonstrated to activate proteinase-activated receptor 1 (PAR_1) (19).

*Corresponding author. kyamada@med.nagoya-u.ac.jp
Published online in J-STAGE
doi: 10.1254/jphs.08R04FM